



Reducing uncertainty in seismic assessment of multiple masonry buildings based on monitored demolitions

Panagiotis Martakis¹ · Yves Reuland¹ · Marco Imesch¹ · Eleni Chatzi¹

Received: 26 July 2021 / Accepted: 17 February 2022 / Published online: 20 March 2022
© The Author(s) 2022

Abstract

A significant part of the existing building stock in regions of low to moderate seismic hazard has been designed without modern seismic considerations and is, in the meantime, exceeding its design life span. The assessment of seismic performance poses an engineering challenge, due to unknown material properties, undocumented structural interventions and the scarcity of event-based information. Operational modal analysis has been applied in some cases to verify model assumptions beyond visual inspection. However, masonry buildings exhibit amplitude-dependent stiffness even at very low response amplitudes, raising questions about the validity of such methods. Planned demolitions provide engineers with the opportunity to leverage higher-amplitude vibrations generated during demolition activities to better understand the dynamic behaviour of existing buildings. This paper introduces a Bayesian model-updating framework, which aims at reducing uncertainty in seismic analysis, by fusing dynamic measurements with best-practice structural models. The proposed hybrid framework is applied to nine real masonry buildings, representative of existing residential buildings, as typically encountered in Switzerland, that have been monitored during controlled demolition. A vast reduction in prediction uncertainty is achieved through data-driven model updating, additionally exposing intra- and inter-typological differences in terms of seismic capacity and ductility. In addition, differences between updated model predictions and typical engineering assumptions and generic typological curves are discussed. Overall, this contribution demonstrates, applies and discusses the practical benefits of a straightforward methodology for fusing monitoring data into the seismic evaluation of existing masonry structures.

Keywords Reducing parametric uncertainty · Demolition monitoring · Bayesian model updating · Seismic assessment · Unreinforced masonry buildings · Amplitude-dependent stiffness · Seismic SHM

✉ Panagiotis Martakis
martakis@ibk.baug.ethz.ch

Extended author information available on the last page of the article

1 Introduction

Earthquakes still pose a major threat to the integrity of the built environment, while the vulnerability of existing buildings exposes communities to the risk of functional disruptions and societal consequences. In regions with moderate seismic hazard, existing structures may not be designed according to modern, if any, seismic standards, thus exposing the built environment to the risk of human and financial toll in the case of an earthquake event. Masonry buildings, which dominate the European building landscape (Lestuzzi et al. 2017; Diana et al. 2019c; da Porto et al. 2021), are characterized by an increased seismic vulnerability (D'Amato et al. 2020). In addition, when only limited damage data is available for informing heuristic vulnerability predictions, a model-based approach for predicting earthquake risk is required. However, it is financially and technically infeasible to systematically evaluate building-specific risk. In addition, many sources of uncertainty, such as the seismic hazard, material properties and foundation impedance undermine a rapid and reliable assessment of specific buildings.

In the past decades, Seismic Structural Health Monitoring, also termed as S²HM, emerged as a multi-disciplinary field that enables the use of monitoring data for structural evaluation prior to and rapid loss assessment tasks after seismic events (Limonelli et al. 2019; Çelebi 2019; Soyoz 2019). In this context, the use of ambient-vibration (AV) monitoring as a data source to identify modal properties has gained popularity for reducing the parametric uncertainty of structural-behavior models (Çelebi et al. 2019; Foti et al. 2012; Sabia et al. 2015; Snoj et al. 2013). AVs are generated by environmental sources, such as wind, micro-tremors, or human activity, like traffic, and are characterised by an almost flat broadband frequency spectrum and very low amplitudes of vibration. Standoli et al. (2021) showed the possibility to reduce uncertainties of orthotropic masonry formulations with AV measurements on a historic masonry tower using surrogate models, getting good agreement with the expert opinion of the vertical stiffness distribution. In addition, changes in modal properties have been fused with models to assess the efficiency of seismic retrofits of existing buildings (Ercan 2018; Michel et al. 2018b) and post-earthquake building capacity (Reuland et al. 2017; Soti et al. 2020). AV-based model-updating has helped to derive the parameter values that provide the best fit to the measured data (Torres et al. 2017; Girardi et al. 2021; Standoli et al. 2021), or implementing probabilistic model-updating approaches (Reuland et al. 2017; Song et al. 2019a; Bartoli et al. 2019). Although some limitations have been reported regarding the assumptions underlying uncertainty (Tarantola 2006; Reuland et al. 2017; Pai et al. 2019), Bayesian model-updating (BMU) provides a powerful and widely applied probabilistic tool to solve inverse data-interpretation problems (Beck and Au 2002; Behmanesh et al. 2015; Straub and Papaioannou 2015). However, such approaches are building-specific, while no comparative study on the effect of model-updating on the seismic analysis results across multiple monitored masonry buildings exists to date. In addition, modal properties depend on the amplitude of vibration (Ceravolo et al. 2017; Astorga et al. 2018; Spina et al. 2019) and are further affected by environmental variability (Nozari et al. 2017; García-Macías et al. 2021), which may undermine model-updating based on AVs. A number of works tackle the influence of varying environmental and operational conditions (EOC), when updating the model parameters (Song et al. 2019b; Martakis et al. 2021a; Limonelli 2010), however less work focuses on amplitude dependency.

While even more simplified modelling approaches exist (Oropeza et al. 2010), the seismic assessment of individual existing masonry buildings often relies on equivalent-frame

(EF) models (Belmouden and Lestuzzi 2009; Nakamura et al. 2016; Manzini et al. 2021). Despite the strongly simplified underlying hypotheses of EF models (Bracchi et al. 2015), their reduced number of mechanical parameters and relatively small computational burden makes them a popular choice in practical applications (Quagliarini et al. 2017), especially in combination with static nonlinear approaches, such as the N2-method (Fajfar and Fischinger 1988; Fajfar 2000; Diana et al. 2019b), which bypass the need for burdensome dynamic nonlinear time-history analyses. In addition to material properties, which may be altered by aging and structural interventions, the seismic response of existing masonry buildings is strongly influenced by the floor slabs. A high vulnerability is for instance found for buildings comprising wooden floors, whose in-plane stiffness and quality of the connections between floors and masonry significantly influence the seismic performance. Structural design codes provide reference stiffness values for timber floors or propose simplified derivation methods for the in-plane stiffness (ASCE/SEI 2017; MBIE-NZSEE 2017).

Measurements of the dynamic behavior of buildings can support the verification and extension of the applicability of such simplified methods to various slab configurations. When the seismic risk is evaluated at a regional scale (Grünthal 1998), buildings are merged into typological classes that share attributes such as construction period, height, material and lateral load-resisting system (Milutinovic and Trendafiloski 2003; Jaiswal et al. 2010; Riedel et al. 2015; Michel et al. 2018a; Crowley et al. 2018). While capacity curves derived for regional typologies are not intended to represent individual buildings, they may provide regional bias, when local construction techniques are ignored (Lestuzzi et al. 2017; Diana et al. 2019a). Although simplified methods for regional seismic assessment exist (Borzi et al. 2008) and have been combined with vibration measurements (Michel et al. 2008), a rigorous framework for data-driven model-updating in order to draw conclusions for multiple buildings in typological context is missing.

This paper employs a BMU framework to leverage modal data extracted from actual and instrumented unreinforced masonry (URM) buildings for seismic assessment. The structural response is measured at various levels of excitation amplitude prior to the development of damage at structural components, allowing for the evaluation of the effect of amplitude-dependence on the model-updating scheme and ultimately on the predicted seismic performance. Realistic data and estimates for nine case studies, falling into four URM building types, are compared. Chapter 2 summarizes the methodological framework for performing modeling, dynamic measurements, model-updating and seismic assessment tasks related to existing masonry buildings under seismic risk. Section 3 starts with the application of the methodology on one of the case studies, before a comparison across all nine real masonry buildings at typological level is conducted. The work concludes with a discussion of the findings.

2 Methodological framework

Dynamic measurements acquired during demolition activities are utilised to perform BMU of a parametric EF model. To reduce the computational burden of BMU, a surrogate model is created, based on the Polynomial Chaos Expansion (PCE) technique. A pool of candidate EF models is created and the seismic evaluation is conducted in a probabilistic manner. The proposed framework is summarized in Fig. 1.

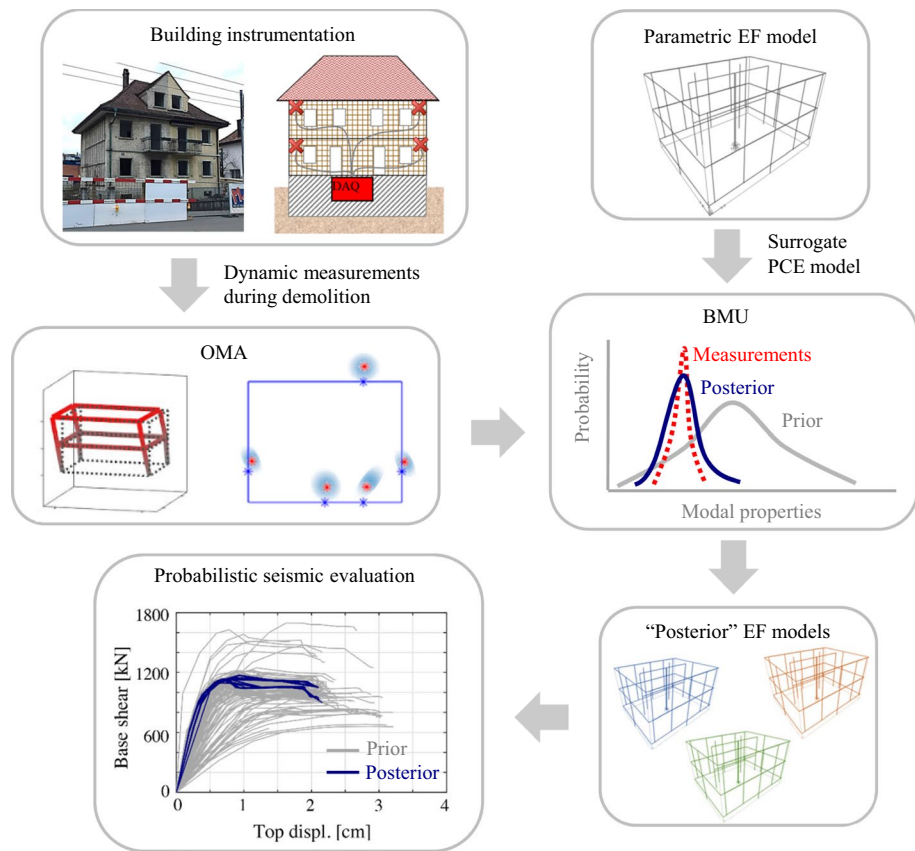


Fig. 1 Illustration of the proposed framework aiming at reducing the uncertainty that inherently characterizes the seismic assessment of URM buildings through the use of dynamic (vibration-based) measurement data

2.1 Modeling principles and unknown parameters

Existing residential URM buildings in Switzerland often exhibit regular, even symmetric, distributions of walls and openings, which justifies simplified modeling approaches, such as the EF modeling method (Lagomarsino et al. 2013; Pasticier et al. 2008). Despite not capturing torsional modes and local failure mechanisms, EF models are selected for their ease of assembly and the possibility of lumping nonlinearity in a computationally efficient manner. The simplification of a three-dimensional orthotropic masonry structure into an EF inevitably includes several strong hypotheses, such as the height of piers, selection of cracked stiffness and distribution of slab loads into vertical structural elements, and there lacks consensus regarding best-practice EF modelling (Bracchi et al. 2015). Nevertheless, the limited computational burden together with the reduced need to define or calibrate unknown mechanical properties of structural materials (Cattari et al. 2015) makes EF models a valuable alternative in practice and when multiple forward simulations are required. In addition, EF models have been shown to realistically capture failure modes of existing masonry buildings (Lulić et al. 2021). The choice of a modelling approach has

an undeniable influence on behavior predictions and may lead to a large scatter given the lack of systematic guidelines for modelling Parisse et al. (2021). The presented framework requires a model that captures the measured dynamic behavior with sufficient precision. In addition, repeated forward simulations are needed. Any modelling technique fulfilling these criteria is deemed acceptable, as the model error is taken implicitly into account in the comparison with measured modal behavior.

Figure 2a illustrates the front view of a typical Swiss URM building. Masonry walls composing the facades are the main contributors to the global lateral stiffness. The regular disposition of openings justify the segmentation of masonry panels into spandrels and piers with overlapping regions. Rigid offsets model the increased stiffness in overlapping regions, as illustrated in 2b. The free length of piers and spandrels forms the deformable part of the wall and is modelled according to the Timoshenko beam theory.

The modulus of elasticity of masonry, E_{mas} , affects the lateral load-resisting behavior both in the elastic and the nonlinear regime (Snoj et al. 2013), while depending on the local and historical material availability and construction practices. In the absence of sufficient documentation and experimental data, structural codes provide broad ranges of possible values for the elastic masonry properties (Ministero delle Infrastrutture e dei trasporti 2018; OPCM 2003). To accommodate this uncertainty, a uniform range between 1 and 7 GPa is considered. These values refer to uncracked conditions, while a reduction factor equal to 50% is considered to account for cracking of masonry during seismic events (CEN 2005; Lang and Bachmann 2004; SIA 2017).

The nonlinear behaviour of masonry is lumped into hinges at the edges and in the middle of the elastic parts. A schematic representation of the hinge positions and capacity curves are given in Fig. 2b and c. The strength criteria for the nonlinear hinges are defined according to Lagomarsino et al. (2013) and are reported in Table 1. The

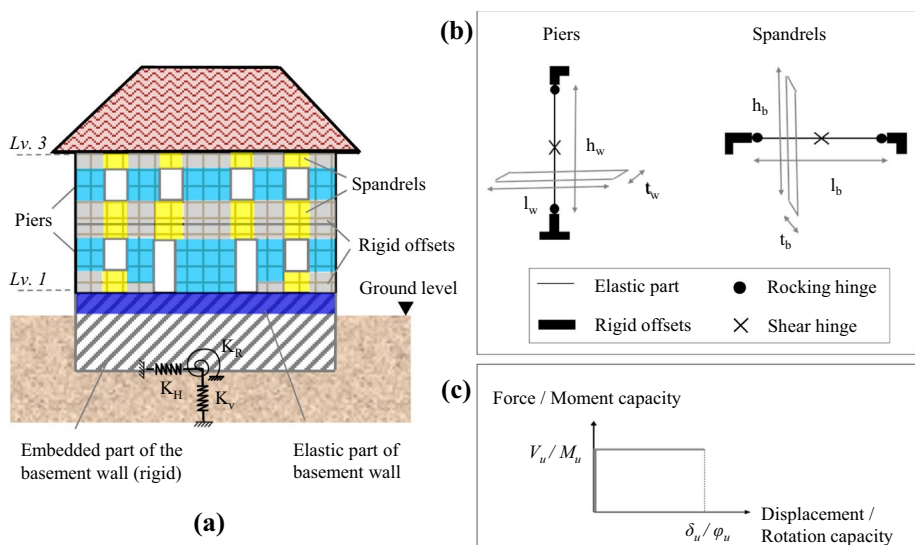


Fig. 2 Equivalent-frame modeling principles: **a** Masonry segmentation to spandrels, rigid offsets and piers. The soil impedance is modelled through equivalent linear springs according to Gazetas (1991). **b** Schematic representation of hinge positions in spandrels and piers. **c** Capacity curve for moment and shear hinges

Table 1 Equivalent-frame model: strength criteria according to Lagomarsino et al. (2013)

Failure	Element	Yield strength	Notes
Rocking	Piers	$M_u = \frac{Nl_w}{2} \left(1 - \frac{N}{0.85f_d l_w t_w}\right)$	f_d : compressive strength l_w : wall length t_w : wall thickness N : acting axial force
	Spandrels	$M_u = \frac{H_p h_b}{2} \left(1 - \frac{H_p}{0.85f_{hd} h_b t_b}\right)$	f_{hd} : compressive strength h_b : spandrel height t_b : spandrel thickness $H_p = 0.4f_{hd} h_b t_b$
Shear	Piers	$V_u = \frac{1.5f_{vd} l_w t_w}{b} \sqrt{1 + \frac{N}{1.5f_{vd} l_w t_w}}$	f_{vd} : masonry shear strength $b = h_w/l_w$ with $1 \leq b \leq 1.5$ h_w : pier elastic height
	Spandrels	$V_u = h_b t_b f_{vd}$	

compression strength of masonry in the vertical direction is considered linearly related to E_{mas} , as prescribed in the Swiss building codes (SIA 2017):

$$f_k = E_{mas}/1000 \quad (1)$$

In the absence of specific guidelines regarding the compression strength in the horizontal direction, it is assumed that $f_{hk} = 80\%f_k$. The shear strength of masonry is considered fixed and equal to 0.2 MPa. For the seismic assessment, compression and shear strength properties are reduced by a safety factor equal to 2 (SIA 2017). The maximum displacement that each structural element can sustain is defined through the ultimate drift, δ_u , which is set equal to 0.4%, in accordance with the Swiss standards (SIA 2017).

The structural elements are modelled up to the level of the last slab. All elements above this level (level 3 in Fig. 2a), including attic storeys, inclined roofs and gable walls, are considered non-structural and only their mass are accounted for (q_{top}). Non-structural elements and live loads are modelled as an uniformly distributed mass acting on all slabs of the building (q_{slabs}). The bounds of the corresponding uniform distributions are reported in Table 2. When performing the seismic assessment, an additional distributed mass equal to 2 kN/m^2 , representing the live loads encountered during in-service conditions, is applied to all accessible slabs of the building.

The slabs are modelled as membrane elements, contributing to the redistribution of the lateral forces and displacements. The self-weight of the slab, as well as all additional vertical loads, are directly assigned to the bearing elements. For buildings with stiff floors, such as reinforced concrete (RC) and composite slabs, the loads are distributed equally to both directions, while for the case of flexible wooden floors, 70% of the floor mass is applied to the strong and 30% to the weak direction. Homogeneous concrete slabs are modelled with their true thickness and typical properties ($E_c = 30 \text{ GPa}$, $\nu = 0.2$, $\gamma_c = 24 \text{ kN/m}^3$). For timber slabs, orthotropic membrane elements with a fixed thickness equal to $t_{eq} = 20 \text{ cm}$ are considered. The equivalent elasticity modulus parallel to the timber beams and the equivalent unit weight are calculated using Eqs. 2 and 3:

Table 2 Equivalent-frame model: prior ranges for uncertain parameters

Property	Unit	Min.	Max.
q_{slabs}	kN/m ²	0	1
q_{top}	kN/m ²	2	5
E_{mas}	GPa	1	7
w_{mas}	kN/m ³	14	18
v_{mas}	—	0.1	0.3
E_{tim}	GPa	7	15
w_{tim}	kN/m ³	3	9
A_{tim}	m ² /m	0.05	0.1
$G_{tim,eq}$	MPa	5	50
v_{tim}	—	0.1	0.3
w_{tim}	kN/m ³	3	9
$G_{soil,eq}$	MPa	10	200
$v_{soil,eq}$	—	0.15	0.35
$w_{soil,eq}$	kN/m ³	14	20

$$E_{tim,eq} = \frac{A_{tim} \cdot E_{tim}}{t_{eq}} \quad (2)$$

$$w_{tim,eq} = \frac{A_{tim} \cdot w_{tim}}{t_{eq}} \quad (3)$$

where A_{tim} refers to the unit cross-section of timber beams in the lateral direction (m^2/m) and E_{tim} and w_{tim} refer to the elasticity modulus and the unit weight of timber material. The unit cross-section of timber slabs in the main direction depends on the cross-section and the average inter-beam spacing. Based on field observations in the studied buildings, the envelop of the unit cross-section of timber beams is considered variable in the range reported in Table 2. Wide bounds for E_{tim} and w_{tim} are considered, in order to account for material variability and changes in construction techniques (see Table 2).

The axial floor stiffness in the weaker direction is also uncertain with bounds of an order of magnitude lower than in the strong direction. The equivalent shear modulus of timber slabs ($G_{tim,eq}$) substantially affects the in-plane flexibility and thus, the modal shapes and the transfer of horizontal loads. Practical suggestions for an equivalent shear modulus of timber slabs (MBIE-NZSEE 2017; ASCE/SEI 2017) are undermined by changing construction practices and historic material availability. Consequently, a wide range, from 5 to 50 MPa, is considered for the equivalent shear modulus of timber slabs.

The EF model includes all structural elements above the ground level, considered as the clamping horizon of the structure. Existing masonry buildings in Switzerland often include a half-buried underground concrete floor, as illustrated in Fig. 2a. In addition to higher stiffness and strength capacity of concrete when compared to masonry, the amount and size of openings in this floor are significantly reduced compared to the masonry superstructure. Therefore, no damage is expected to develop at this floor and no nonlinear hinges are placed within the concrete elements. As shown in Fig. 2a, only the part above ground of the semi-underground walls is modelled with frame elements.

The bottom points of the structure are considered rigidly connected to the geometrical centre of the foundation, where the boundary conditions are applied. In order to account for the impedance of the soil, the boundary conditions are modelled through three translational and three rotational linear springs, in accordance with the analytical formulations proposed by Gazetas (1991) and experimentally validated by Martakis et al. (2017). The foundation impedance comprises a static and a dynamic component, which depend on the geometry of the foundation footprint, the embedment depth and the equivalent linear shear modulus of the soil, which is rarely known with sufficient confidence. A wide range of is therefore adopted for the equivalent G-modulus of soil, as reported in Table 2.

2.2 Identification of modal properties

EF models expectedly suffer model bias, due to the inherent modeling assumptions, such as the idealized representation of the bearing elements as frame objects. The added uncertainty from model parameters, described in the previous section, eventually lead to a large scatter in the predicted behavior. Modal identification of dynamic measurements allows for an approximate evaluation of the model bias by comparing predicted and measured response ranges, while model-updating techniques lead to calibration/reconfiguration of the employed model, with a reduction of the associated uncertainties. While highly sensitive sensors allow for the extraction of the modal properties from AVs, the validity of the inferred properties is debatable, as the stiffness of masonry depends on the loading amplitude and shows a reversible nonlinear behaviour, even in the theoretical linear elastic regime (Michel et al. 2011; Song et al. 2019b; Guéguen et al. 2020). This effect has so far been attributed to breathing cracks in composite inhomogeneous materials and not to permanent damage, as the initial stiffness is recovered, when the vibrational amplitude decreases. Additionally, the soil stiffness is known to be strain-dependent (Benz 2007; Martakis et al. 2017). As soil strains increase with the amplitude of vibration, the soil stiffness, and consequently the equivalent stiffness of the soil-foundation-structure system, depend on the response amplitude as well. The EF models presented in this work intend to simulate the behaviour of URM structures, while taking into account soil-structure interaction effects. While modal properties obtained from AVs are extensively used for inverse updating of linear elastic models, criticism has arisen for their overestimation of the equivalent elastic stiffness properties (Martakis et al. 2021a; Michel et al. 2011; Song et al. 2019b). In the absence of strong ground motions, demolition-generated vibrations offer an opportunity to record the real dynamic response of buildings under vibration amplitudes higher than AVs. These data enable a probabilistic estimation of the elastic properties, including the effect of amplitude. In addition, higher-than-ambient vibrations serve as a reference for quantifying this effect on the dynamic response in the, commonly assumed, linear elastic regime.

A framework for amplitude-dependent modal identification, based on monitored demolition activities, has been proposed (Martakis et al. 2021a, b). Following this framework, a low-cost sensor configuration comprising multiple triaxial accelerometers (ADXL 354) has been deployed in nine URM buildings undergoing planned demolition. A network of 7 to 10 sensors has been distributed along the elevation and floor plan of the buildings prior to the beginning of the demolition process. The data acquisition was conducted by means of a National Instruments cDAQ-9188 at a sampling rate of 1720 Hz. The buildings were monitored continuously throughout the demolition process, up to the point where severe structural damage compromised the global structural integrity, leading to datasets of 15

minutes for the smallest and 3 hours for the largest building. Weather conditions were stable throughout the duration of measurements and thus, environmental conditions are considered not to alter material properties. A camera captured the damage-condition of the building.

In all case studies, the demolition has been conducted with an excavation shovel, starting from the top of the structure with the removal of non-structural elements, such as roof tiles and support, and progressively reaching the top slab and the supporting masonry walls. Non-structural elements from the interior of the building were removed beforehand. During demolition, buildings are subjected to hits and pulls of arbitrary direction and intensity, providing a rich variety of impulse responses. The duration of the contact is negligible and thus, transient phenomena due to the frequency content of the excitation are irrelevant. Although excitation amplitude, location and direction cannot be measured directly, the intensity metrics of the building response can be utilized to cluster the response impulses into groups of similar amplitude. The data used for the purposes of model updating are limited to the vibrations generated during preparation works and demolition activities at the roof-top level, prior to the formation of visible damage on structural elements. Monitoring this process provided a rich amount of vibration recordings at amplitude levels over an order of magnitude higher than due to AVs.

Figure 3a comprises a schematic representation of a typical demolition-monitoring configuration, where sensors are attached to the masonry walls at the floor levels. In Fig. 3b a schematic representation of a characteristic acceleration recording is shown, as well as the identified impulses, after applying a Savitzky-Golay smoothing filter (Schafer 2011), and the distribution of the extracted impulses with respect to amplitude, by considering as amplitude metric the root-mean square (RMS) acceleration of the impulse response. Initially, a baseline identification is conducted based on 10 to 20 minute AV recordings

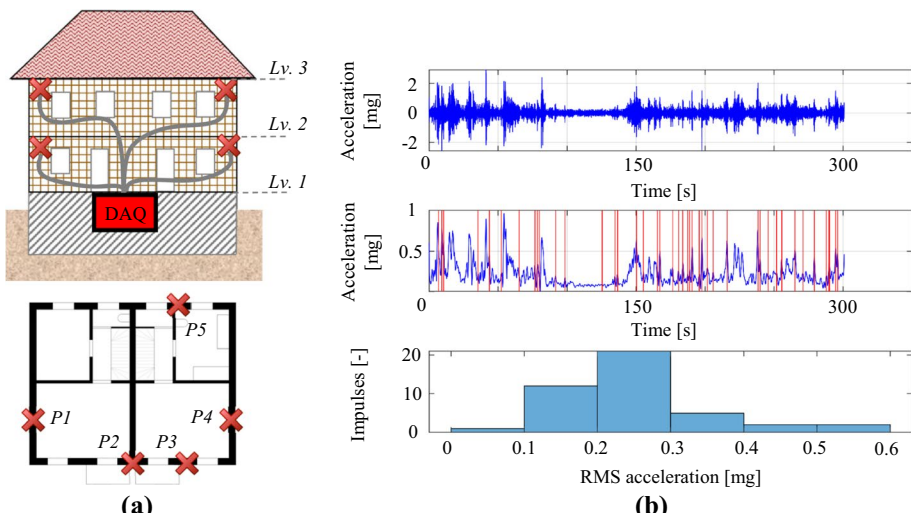


Fig. 3 Overview of dynamic measurements recorded during demolition for the case of building MW2 (Appendix A): **a** Schematic representation of typical sensor configuration for the monitoring of a masonry building undergoing demolition. **b** Characteristic dynamic response, the filtered signal and the impulse identification and distribution in terms of RMS acceleration amplitude of vibration data measured on a real building

prior to the beginning of the demolition process, by applying a covariance-based Stochastic Subspace Identification algorithm (Peeters and De Roeck 1999). The modal properties identified under ambient conditions are then considered as a reference for subsequent identification, based on the structural response during demolition. The dynamic response of the buildings during demolition moves away from the “ambient” response (meaning response due to a broad-spectrum input) and, instead, resembles a sequence of impulse responses due to unknown excitation in terms of amplitude, position and direction. Based on this assumption, which stems from observations in the response signals and cannot be verified explicitly, each impulse response is analysed individually and the modal properties are identified by means of the Eigensystem Realization Algorithm (ERA) Juang and Pappa (1985), since this algorithm was originally developed specifically for application with impulse response data. Due to the short duration of the impulses (1 to 3 seconds), their arbitrary input (location, direction and amplitude) and the inherent measurement noise, the operational modal analysis procedure is only able to identify the excited modes during the studied impulse. In order to encounter known issues of the ERA algorithm, related to the selection of the model order (Civera et al. 2021), a grid search is conducted for each analysed impulse response, by considering model orders ranging between 2 and 20. In order to limit identification to the global modal shapes and to ensure consistency of the identified modal properties, three criteria, evaluating the goodness of fit between ERA predictions, reference identification and the real response, have been implemented, as described in previous work of the authors (Martakis et al. 2021a). Figure 4a illustrates a characteristic distribution of the identified frequencies for the two translational modes of an URM building, based on the extracted impulse responses, compared with the reference identification. Figure 4b illustrates the identified modal shapes based on the reference identification and

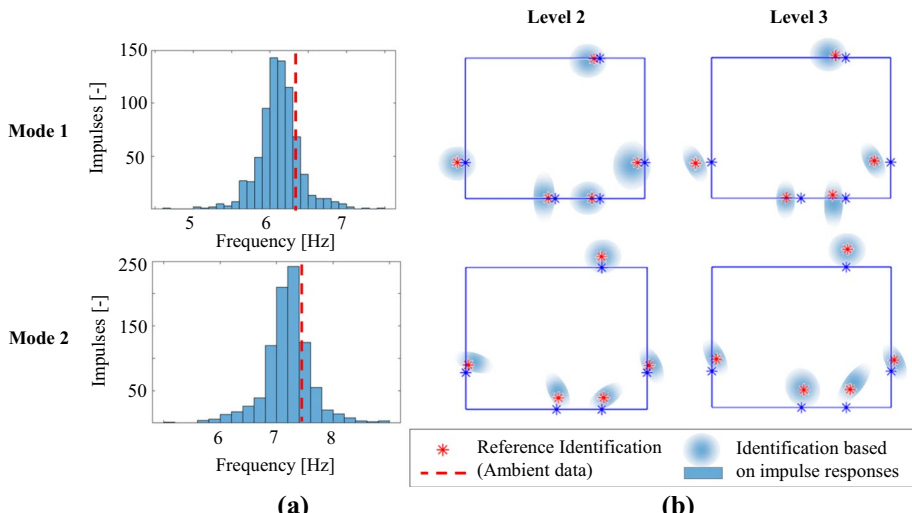


Fig. 4 Schematic representation of modal identification for the case of building MW2 (Appendix A): **a** Identified frequencies of the translational modal shapes based on impulse responses under demolition hits. The dashed line indicates the point estimate based on ambient recordings (reference identification). **b** Identified modal shapes based on ambient recordings and impulse responses. The initial sensor positions are marked on the outline of the building

impulse responses. The identified distributions are subsequently considered for the update of the EF model.

2.3 Metamodeling and sensitivity analysis

Given a set of independent input variables X a computational model M approximates the response vector Y as follows:

$$\hat{Y} = M(X) \quad (4)$$

In the absence of measurement data, it is impossible to evaluate the quality of the physics-based model, while the effect of parametric uncertainties on the predicted response is often neglected. Probabilistic approaches propagate parametric uncertainties to the prediction outcomes, but come at the cost of multiple model evaluations, which in most cases are computationally burdensome. To reduce the time required for multiple forward model evaluations, surrogate models substitute the physics-based model with a much faster metamodel, capable of approximating the desired response with sufficient accuracy. Polynomial chaos expansion (PCE) is a highly efficient metamodeling technique, which relies on the spectral representation of a computational model on a suitable basis of polynomial functions:

$$\hat{Y} = M(X) \approx M^{PCE}(X) \sum_{a \in \mathbb{N}^M} y_a \psi_a(X) \quad (5)$$

where $\psi_a(X)$ are multivariate polynomials orthonormal with respect to the probability density function of the input space and $y_a \in \mathbb{R}$ refers to the corresponding coefficients. In most realistic applications, a finite number of polynomials is considered and thus a truncation scheme, for instance based on a maximum polynomial order, or the hyperbolic (or q-norm) truncation scheme is applied (Blatman 2009). For the present application, all uncertain parameters of the input space are modeled as uniformly distributed variables, thus Legendre polynomials are considered as basis (Marelli and Sudret 2019). The q-norm truncation scheme is selected with $q = 0.5$ and the maximum polynomial degree is set equal to 8. Based on these assumptions, the surrogate model is created in the uncertainty quantification software UQlab, developed at ETH Zurich (Marelli and Sudret 2014). Initially, a set of 2000 samples from the uncertain input space described in Table 2 is selected for the training of the surrogate model, by implementing Latin hypercube sampling (McKay et al. 1979). An additional set of 200 random samples is drawn for validation purposes. In order to carry out the simulations for all input samples, a set of three-dimensional EF models is generated in the commercial software CSI SAP 2000 (v.23). The generated output in terms of modal frequencies and displacements enables training of the surrogate PCE model. The trained model is validated against the EF model predictions in terms of absolute residuals:

$$Error = M^{EF}(X) - M^{PCE}(X) \quad (6)$$

Additionally, the compatibility of the produced modal shapes is assessed by means of the modal assurance criterion (MAC).

With a sufficiently accurate and computationally efficient PCE model, a global sensitivity analysis can be conducted to identify the input parameters that affect the modal response substantially. Considering independent input variables, the first-order Sobol's index expresses the relative contribution of each input variable X_i to the total variance

(Sobol 2001). The analytical derivation of Sobol's decomposition for truncated PCE has been introduced by Sudret (2008), reducing the computational cost for the calculation of Sobol indices for PCE metamodels. The sensitive analysis is conducted in the uncertainty quantification software UQlab, developed at ETH Zurich Marelli and Sudret (2014).

2.4 Bayesian framework for model updating

Once the parameters with a significant influence on modal properties are identified, a parametric analysis is conducted in order to illustrate the effect of input uncertainty on model predictions. Probabilistic approaches can be further deployed in order to assess the distribution of the predicted performance or the structural reliability. However, model bias and parametric uncertainty are still present when probabilistic methods are used for the seismic assessment of existing buildings. To this end, the modal properties that are identified through the dynamic measurements described herein can provide a reference of the real building behavior, which can be utilized to more reliably update the computational model. In deterministic approaches, the updating task is formulated as an optimization problem with an objective function that minimizes the discrepancy between the predicted and the measured modal properties. The objective functions typically include a frequency fit criterion (FF) or a combined frequency and modal shape fit criterion (FSF):

$$FF = \frac{1}{N} \sum_{i=1:N} \left\{ 1 - \left| \frac{f_i^{id} - f_i^M}{f_i^{id}} \right| \right\} \quad (7)$$

$$FSF = \frac{1}{N} \sum_{i=1:N} \left\{ \left(1 - \left| \frac{f_i^{id} - f_i^M}{f_i^{id}} \right| \right) \cdot w_i^f + MAC(\phi_i^{id}, \phi_i^M) \cdot w_i^\phi \right\} \quad (8)$$

where N is the number of modes considered for the update, f_i^{id} and f_i^M refer to the identified and predicted frequency for the i^{th} mode and ϕ_i^{id} and ϕ_i^M refer to the identified and predicted modal shapes for the i^{th} mode. The coefficients w_i^f and w_i^ϕ correspond to the weight factors for mode i , both of which will be further considered equal to 0.5 for all modes. Although such approaches offer an “optimal” point estimate for the uncertain properties, the discrepancy between measured and predicted behavior, due to measurement errors or model bias, is not accounted for. Additionally, considering that measurements provide only a scarce representation of the system response, point estimates may be prone to overfitting, while there is no information regarding other parameter combinations that potentially yield high fit scores and may therefore be a viable explanation of the measured behavior.

BMU provides posterior distributions of the input parameters X for which the fit between model predictions and the available data is compatible with uncertainties that are presents in both the measurements (data) and the modeling process (see Fig. 5a). The measured response Y can be linked to the model prediction as follows:

$$Y = M^{PCE}(X) + \varepsilon \quad (9)$$

where ε describes the discrepancy between the observations Y and the model prediction due to measurement or modelling inaccuracy. Assuming that model bias can be ignored, this term is represented as an additive Gaussian noise with zero mean and a diagonal covariance matrix:

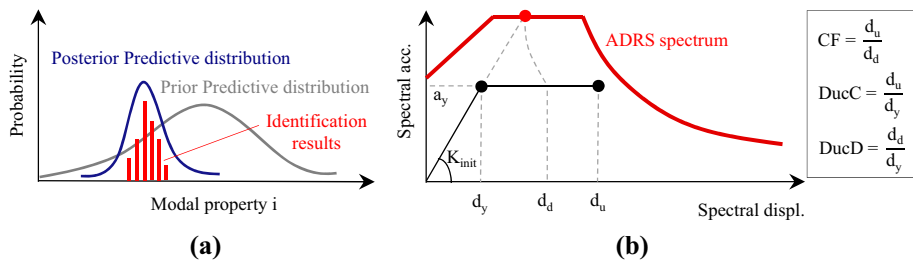


Fig. 5 **a** Schematic illustration of Bayesian inverse analysis, **b** Bilinear approximation of pushover curves and definition of seismic performance metrics

$$\boldsymbol{\varepsilon} \sim \mathcal{N}(\mathbf{0}, \boldsymbol{\Sigma}) \quad (10)$$

For N independent observations ($\mathbf{Y} = \mathbf{y}_1, \dots, \mathbf{y}_N$) and M identified modal properties ($\mathbf{y}_i = y_{ij}, \dots, y_{iM}$), each diagonal term jj is considered a random variable with uniform distribution in the range: $[0, \sigma^2(Y_j)]$, which can be inferred through the subsequent BMU. All identified modal properties (frequencies and modal shapes) for the i^{th} observation (\mathbf{Y}_i) are considered as equally weighted realizations of independent Gaussian distributions with mean values estimated from $M^{PCE}(\mathbf{X})$ and covariance matrix ($\boldsymbol{\Sigma}$). The likelihood is estimated from the multivariate Gaussian distribution, which is formed as the product of the above marginal Gaussian distributions and can be formulated as:

$$\mathcal{L}(\mathbf{X}, \mathbf{Y}) = \prod_{i=1}^N \prod_{j=1}^M \mathcal{N}(y_{ij} | M^{PCE}(\mathbf{X}), \boldsymbol{\Sigma}) \quad (11)$$

In order to obtain an approximation of the posterior distribution, 5000 Markov chain Monte Carlo (MCMC) simulations are performed after applying the Affine Invariant Ensemble Algorithm (AIES) Goodman and Weare (2010) for an ensemble of 20 Markov chains. In order to exclude the points generated prior to convergence, the initial 50% of the sample points is discarded (burn-in). The remaining points represent valid samples of the posterior distribution of the uncertain properties. In order to account for changing amplitude levels, the BMU, implemented in the uncertainty quantification software UQlab Marelli and Sudret (2014), is conducted separately for low- and high-amplitude impulse response sets, providing posterior distributions for various amplitude levels.

2.5 Seismic performance evaluation

By applying Latin-hypercube sampling, an independent set of parameter values is drawn from the posterior distributions of the parameter values, obtained using Gaussian inverse updating (see Sect. 2.4). Subsequently, with the reduced parametric uncertainty of the posterior distributions, the seismic performance can be assessed more precisely. Within this framework, seismic assessment is performed using a static nonlinear procedure based on displacement-based pushover analysis of the three-dimensional EF models. The displacement is imposed independently in both orthogonal directions, proportional to the respective translational modal shapes on all nodes of the EF model.

The average displacement of all nodes at the top level and the shear force at the foundation level define the pushover curves. This pushover curve is then simplified into a bilinear capacity curve, using the steps defined by the European standards (CEN 2005). Following the N2-method (Fajfar and Fischinger 1988; Fajfar 2000), the bilinear curves are transformed into equivalent single-degree-of-freedom (SDOF) representations, as shown in Fig. 5b. The bilinear curves, that are used to derive the seismic performance with the static-nonlinear approach, are thus defined through three parameters: the yield displacement (d_y), the yield acceleration (a_y) and the ultimate displacement (d_u). The displacement demand (DispD), which is associated with the site-specific seismic hazard spectrum, is defined as the intersection of the extended linear part of the equivalent SDOF bilinear capacity curve and the design spectrum. The latter should be formulated in the acceleration-displacement response spectrum format (ADRS), following the N2-method, which has some known shortcomings (Diana et al. 2018). Updated model parameters play a key role in this part of the analyses, as the imposed nodal displacements rely on the modal shape and the initial stiffness, both depending on uncertain parameters that are updated using measurement data.

Based on the aforementioned response values, typical seismic performance metrics can be defined to quantify the expected seismic performance of the studied structure, as formulated in Fig. 5b. The ductility capacity (DucC) is a vulnerability metric, defined as the ratio of the ultimate and the yield displacement. Higher values of DucC reflect the capacity to redistribute lateral loads and sustain larger displacements before the global collapse of the structure. The compliance factor (CF), which forms the most widely used performance metric, is defined as the ratio of the ultimate displacement and the displacement demand. CF values below 1 indicate that the structure cannot sustain the design requirements. Thus, CF provides an estimate of the life-safety margin of a building with respect to earthquakes with a code-defined return-period for the site of interest. Finally, the ductility demand (DucD) is defined as the ratio of the displacement demand and the yield displacement. This metric expresses the level of nonlinearity the structure is expected to sustain, when undergoing an earthquake that follows the design spectrum. The DucD offers insights into the level of damage that is expected to be sustained by a structure. The three selected performance metrics provide a comprehensive view of the global structural performance for a specific seismic scenario. For the purposes of this analysis, local failure modes and the effect of higher modes are neglected.

3 Case studies

The introduced framework is applied to nine real URM buildings erected in Switzerland between 1898 and 1960. Table 3 summarizes the typological classification of the studied buildings, based on the EMS-98 classification scheme (Grünthal 1998), further enriched by Lagomarsino and Giovinazzi (2006). While the studied buildings demonstrate distinctive characteristics, they can be attributed to three main typological classes, namely timber floor (low- to medium-rise), RC floor (medium-rise) and composite RC-masonry floor (high-rise) buildings. A comprehensive documentation of geometrical characteristics of all case studies is provided in Appendix A.

The framework, illustrated in Fig. 1, is demonstrated on a single building, MW1, in order to offer the details of the employed model-updating procedure and evaluate the resulting effect on the predicted seismic performance. Observed reversible nonlinearities in

Table 3 Building description, typological classification according to Lagomarsino and Giovinazzi (2006) and identified frequencies of the first two translational modal shapes

ID	Erection	Floors	L_x/L_y [m/m]	Slab	Typology	Freq. 1 [Hz]	Freq. 2 [Hz]
MW1	1927	3	7/7	Timber	M5.w_M	5.9 ($\parallel y$)	6.9 ($\parallel x$)
MW2	1922	3	10/8	Timber	M5.w_M	6.3 ($\parallel x$)	7.4 ($\parallel y$)
MW3	1928	2	7/7	Timber	M5.w_L	7.8 ($\parallel x$)	10.3 ($\parallel y$)
MW4	1898	4	20/10	Timber	M5.w_M	3.2 ($\parallel y$)	4.5 ($\parallel x$)
MC1	1930	3	8/13	RC	M6_M-PC	6.1 ($\parallel x$)	7.3 ($\parallel y$)
MC2	1948	4	17/11	RC	M6_M-PC	7.1 ($\parallel x$)	7.9 ($\parallel y$)
MC3	1948	4	35/11	RC	M6_M-PC	7.2 ($\parallel y$)	7.5 ($\parallel x$)
MC4	1960	5	18/9	RC	M6_M-PC	5.0 ($\parallel y$)	6.5 ($\parallel x$)
MR1	1930	6	23/10	RC-masonry	M5_H	3.3 ($\parallel y$)	3.9 ($\parallel x$)

The mode directions refer to the global axes defined in Fig. 6c for building MW1 and in Appendix A for the rest of the buildings

the dynamic response are discussed and various updating approaches are compared. Subsequently, the framework is applied to all case studies to draw conclusions from a typological perspective. Ultimately, the value of data-informed seismic evaluation is assessed, by comparing the uncertainty margins of the predictions, before and after model-updating. The narrow posterior ranges allow for a meaningful comparison in terms of seismic performance of structures belonging into the same typological class. For the first time, real data of a population of masonry buildings are utilised in order to reduce epistemic uncertainty in URM modeling and provide the basis for the development of building classification schemes that are based on updated seismic performance.

3.1 Individual building analysis

Building MW1 was built in Switzerland in 1927 and represents a medium-rise masonry structure with timber floor slabs (see Fig. 6). The building geometry is almost symmetric in both directions, with an outer envelope of 7 m × 7 m and a total height equal to 10 m. The external walls are 24 cm thick and are the main contributors to the lateral building stiffness. The internal walls are thinner and support the timber slabs, that are spanning parallel to the y-axis.

3.1.1 Modal identification

Prior to planned demolition, sensors are placed at all floor levels at the marked positions (see Fig. 6c), in order to capture the global dynamic response. The modal characteristics, identified based on AV measurements, provide point estimates and are considered as the reference identification. In Table 3 the reference identified modal properties for the first two translational modes are summarized. Axes x , y refer to the direction of the translation with respect to the global axes defined in Fig. 6a and in Appendix A.

Impulse responses allow for the identification of modal characteristics at different amplitude levels. As explained in Sect. 2.2, the studied impulses are restricted to the vibrations recorded during demolition activities prior to the development of visible damage on structural elements. Previous work by the authors has concluded that the maximum

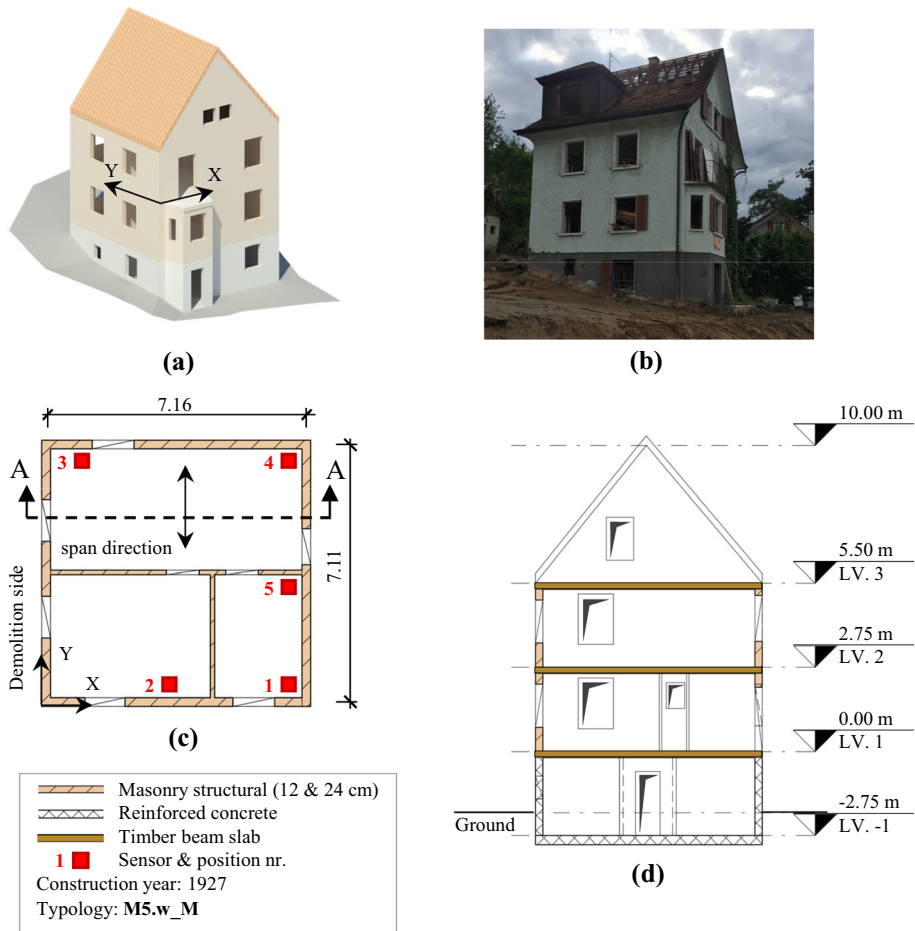


Fig. 6 Case study MW1: **a** 3D-rendering of the studied structure, **b** typical ground floor including the sensor positions, **c** cross-section of the building

amplitude of the impulse responses is over an order of magnitude lower than the numerically predicted yield point, while the observed nonlinearities due to increased amplitude are reversible and do not relate to permanent damage (Martakis et al. 2021a).

Figure 7a illustrates the identified value for the first frequency, normalised to the reference value, for each individual impulse response. Marker sizes correspond to the amplitude level, defined as the RMS acceleration of the impulse response, while the horizontal axis corresponds to real time. The impulses are empirically clustered into two intensity classes by defining a threshold at 0.4 mg. The dashed lines correspond to moving averages for low and high amplitude impulses. Higher amplitude impulses yield consistently lower frequency values, while the low amplitude identification results show no significant variation over time, indicating reversible softening due to increased response amplitude, which cannot be attributed to permanent structural damage. In Fig. 7b the relation between the identified frequency corresponding to the first mode and the response amplitude is plotted: the dots indicate the mean and the shaded regions the 25th and 75th percentiles respectively.

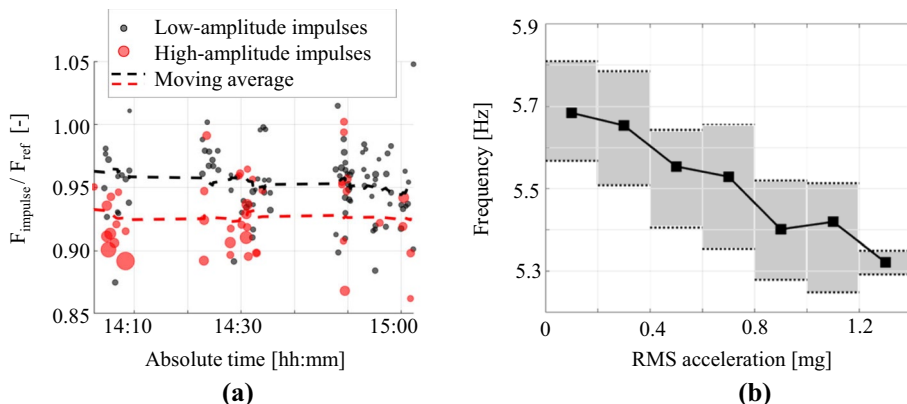


Fig. 7 Influence of the amplitude of shaking on the modal properties: **a** Identified frequency of the first mode for each impulse response during demolition, normalised to the reference value from AVs. The horizontal axis refers to the real timestamp and the size of the markers to the amplitude of each impulse. Impulses with RMS acceleration below and above 0.4 mg are classified to low- and high-amplitude respectively. **b** Identified frequency for increasing amplitude. Mean and 25/75-percentiles are derived for amplitude bins of 0.2 mg

The relation appears to be almost linear, reaching a frequency drop up to 10% compared to the reference value. This amplitude-dependent reversible softening exposes elastic nonlinearities in the, commonly assumed, linear elastic regime, that can be attributed either to the strain dependency of the soil stiffness and/or to temporary crack opening in masonry (breathing cracks). The coefficient of variation of the identification results in each amplitude bin does not exceed 3% in all cases, which is deemed acceptable for field measurements during higher-than-ambient excitation.

3.1.2 Surrogate modeling and sensitivity analysis

In order to reduce the computational cost of the model-updating, a PCE based surrogate model is trained on a set of 2000 EF configurations and evaluations, following the procedure described previously. An additional set of 200 EF samples is considered for the validation of the trained model. Figure 8a and b report the distributions of the absolute residuals between the EF and PCE models in terms of modal frequencies and modal shapes (normalised to the maximum displacement) for the first two modes. The distributions are given in the form of boxplots, encoding the statistical mean, the 25th and 75th percentiles and the extreme values of the distribution. Both frequencies and modal displacements show 0 mean, indicating no bias, and very narrow variability. For the frequencies, the extreme error values do not exceed 0.2 Hz, less than 5% of the identified frequency. The modal displacement error shows low variability in most cases, with minor exceptions with regard to the second mode, where maximum absolute error is not always negligible, implying the existence of outliers. By computing the MAC between the EF and the PCE predicted modes, the lowest fit yields 99% and 95% for the first and second modes respectively, confirming that the outliers in the prediction of modal shapes do not happen simultaneously and do not compromise the predictive performance of the surrogate model. Figure 8c and d illustrate the direct comparison of the modal shape predictions between the PCE and the EF model for the case of minimum MAC value. As it can be observed, in the second

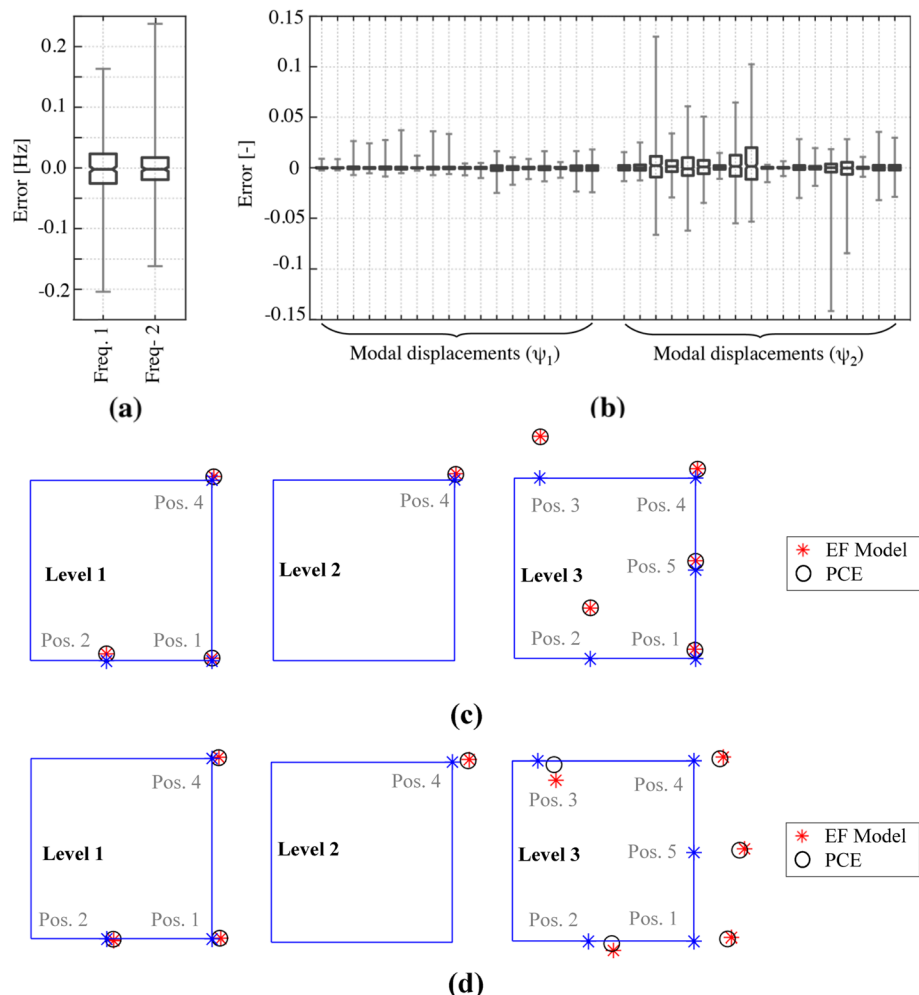


Fig. 8 Comparison of Polynomial Chaos Expansion model predictions (PCE) with respect to EF model: error distribution for the first two natural frequencies **a** and the corresponding modal shapes **b**, direct comparison of the modal shape prediction for the first **c** and second mode **d**

mode the PCE model slightly underestimates the displacements parallel to the global translation direction at the top floor, whereas at position 3 the PCE model partially misses the out-of-plane component of the modal displacement. Given that this comparison refers to the worst fit between the two models and that out-of-plane and torsional behaviour are anyway neglected during the subsequent seismic evaluation through nonlinear static pushover analysis, the surrogate model is deemed to approximate the modal predictions of the EF model sufficiently well.

Subsequently, a sensitivity analysis is conducted by applying the ANOVA method. The first order Sobol indices are computed for all uncertain parameters and identified modal quantities of the first two modes. Figure 9a reports the average values of the Sobol indices considering all modal quantities. The dashed line indicates the assigned threshold of 10%, above which the modal predictions are considered sensitive to the corresponding uncertain parameters and

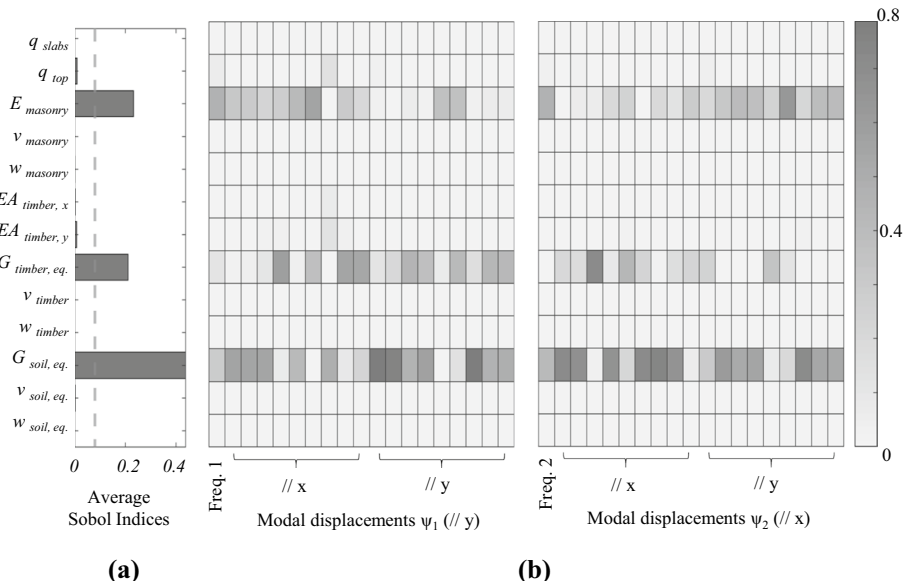


Fig. 9 Sensitivity analysis based on the ANOVA method: **a** Bar plot of the average Sobol values for all modal parameters. The dashed line indicates the threshold, above which the parameters are considered sensitive. **b** Heatmap plot of the computed sensitivity for each modal quantity for the first two modes. The directions of the individual modal displacements and the modal shapes refer to the global axes defined in Fig. 6c

will be updated. In all studied cases, the E_{mas} and the $G_{soil,eq}$ are the most sensitive parameters, while the G modulus of the slab has a significant influence in buildings with flexible floors. Figure 9b illustrates the individual values of the first order Sobol indices for each modal quantity. $G_{soil,eq}$ affects all modal quantities while E_{mas} appears to mostly govern the modal displacements that are orthogonal to the corresponding mode direction. Finally, $G_{tim,eq}$ mostly influences the modal displacements that are parallel to the mode direction, while barely influencing the frequencies. Therefore, neglecting the modal shapes would undermine the identification of $G_{tim,eq}$. Overall, the sensitivity analysis allows to reduce the amount of uncertain properties from 14 (see Table 2) to two or three parameters, depending on the slab stiffness.

The parameters that are retained govern the elastic behaviour of the system and, consequently, the predicted modal quantities. However, these properties are also expected to bear an impact on the predicted seismic performance. Indeed, the E_{mas} influences both the elastic stiffness of the superstructure, and thus the seismic demand, as well as the strength capacity of masonry, according to Eq. 1. In addition, $G_{soil,eq}$ influences the overall stiffness of the system soil-structure-foundation, thereby influencing seismic demand. Finally, $G_{tim,eq}$ affects the redistribution of forces and deformations during lateral loading and, consequently, the global strength and ductility capacity.

3.1.3 Model updating procedure

Initially, an optimization-based approach is applied by implementing the objective functions FF and FSF, formulated in Eqs. 7 and 8. A population of 2000 models, obtained

with Latin-hypercube sampling of the input space, is developed and the fit is computed by comparing the predicted modal properties with the results of the reference identification. The maximum fit reveals the best model representing the optimal calibrated parameters in a deterministic context. Parameter ranges that are associated with high fit-scores can be extracted by the model configurations that yield fit over a fixed threshold. By applying the optimization-based approach, the “optimal” models yield fit scores: 99% and 94%, by considering the FF and FSF criteria (see Eqs. 7 and 8). After setting the acceptable-fit thresholds at 97% and 92% respectively, multiple values for the uncertain parameters are extracted.

BMU allows for a probabilistic estimation of the posterior distribution by utilising the uncertainty distribution of the acquired impulse responses. Figure 10 summarizes the prior and posterior ranges, along with the measured modal quantities in form of boxplots, where the thick lines indicate the range between the 25th and the 75th percentile. Considering the identified modal properties based on the measured data, the coefficient of variation for the first two identified frequencies lies below 3.5%, while the standard deviation for the modal displacements varies between 0.06 and 0.15. Given the short duration of the impulses (1 to 3 seconds), their arbitrary input (location, direction and amplitude) and the inherent measurement noise, the measured variability is deemed reasonable. The prior ranges of the predicted modal properties cover the recorded data, indicating no significant bias between model and measurements. The posterior ranges capture the measured response and thus, justify the narrow posterior ranges of the uncertain properties. Figure 11 summarizes the updated ranges and point estimates for the uncertain parameters based on the optimization approach and the BMU. Both approaches are applied by considering the frequency-fit (FF) and the combined frequency and modal shape fit (FSF). The y-axis is bounded by the prior

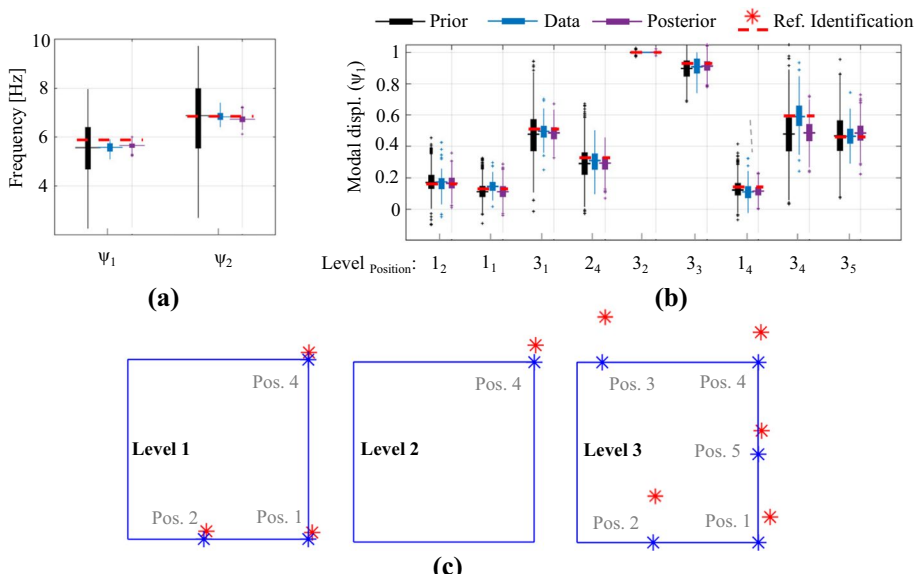


Fig. 10 Bayesian model-updating results: **a** Prior and Posterior ranges of the first 2 characteristic frequencies. **b** Modal displacements of the first mode. The dashed lines indicate the reference identification. **c** Sensor positions and first identified modal shape based on the reference identification. The exact sensor positions are reported in Fig. 6c

limits of each uncertain parameter. The results indicate that even after defining thresholds that are close to the “best fit”, the optimization-based approaches fail to reduce the input uncertainty significantly. Consequently, the accuracy of the point estimate may be considered to be limited, while no remarkable difference in terms of uncertainty is observed after integrating the modal shapes into the updating scheme. BMU provides consistent point estimates of the uncertain properties, when comparing the statistical mean of the posterior ranges of the FF and FSF results. The Bayesian FF approach yields significantly larger uncertainty compared to the FSF, especially with regard to E_{mas} and $G_{soil,eq}$, that are competing stiffness parameters. Considering the modal shapes substantially enriches the fidelity of the update procedure and enables the inference of mutually competing stiffness parameters with paramount importance on the accuracy of model predictions.

In order to evaluate the effect of amplitude on the identified modal properties and, consequently, on the inferred parameters, BMU is applied separately to low and high amplitude impulse responses. Considering the frequency drop reported in Fig. 7b, the amplitude threshold in terms of RMS acceleration is set equal to 0.4 mg. The identified parameter distributions are reported in Fig. 12. All inferred stiffness parameters show low variability and reduce with increasing amplitude. The E_{mas} and $G_{soil,eq}$ demonstrate 12.9% and 9.5% drops respectively, indicating an almost equal contribution of soil and structural stiffness to the amplitude-dependent softening of the structure.

3.1.4 Seismic-capacity predictions

Parameter identification is here pursued with the aim of bounding the prediction uncertainty pertaining to the seismic capacity of the building. Therefore, EF models (see Sect. 2.1) are used to predict pushover curves, which are in turn deployed for spectrum-based predictions of the seismic capacity through the N2-method, as explained in Sect. 2.5. Reducing the uncertainty of the input parameters minimizes the variability of the predicted pushover curves, as shown in Fig. 13a. To facilitate the implementation of the N2-method, the pushover curves are transformed into idealized bilinear curves. The uncertainty reduction in predicted bilinear curves, achieved through data-based model-updating, is reported in Fig. 13c. The scatter in the three quantities defining the capacity curve, namely yield displacement, d_y , ultimate displacement, d_u , and yield acceleration, a_y , is reported using

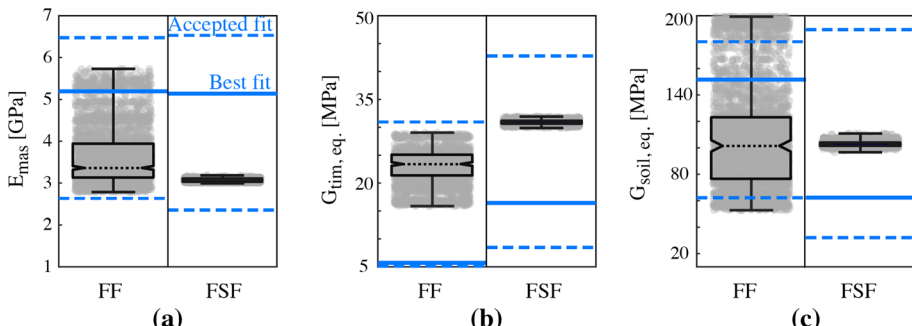


Fig. 11 Posterior ranges and point estimates of **a** E_{mas} , **b** $G_{tim,eq}$ and **c** $G_{soil,eq}$ based on the optimization-based approach (blue color) and the Bayesian inference (black color). The left and the right sides refer to the results for frequency-fit (FF) and the combined frequency- and modal shape-fit (FSF) respectively

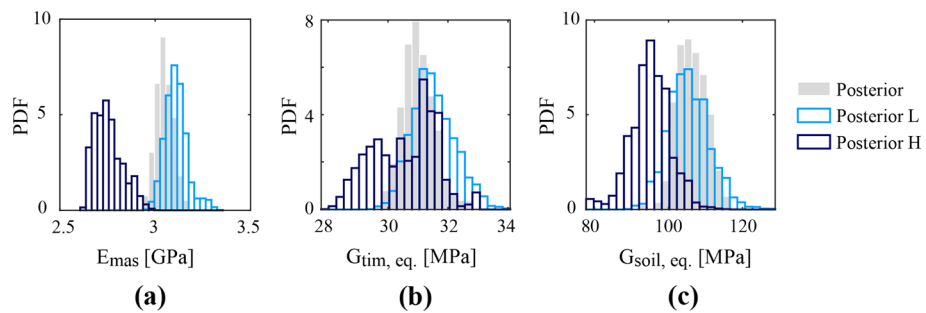


Fig. 12 Posterior ranges of uncertain parameters for Bayesian inverse updating at different amplitude levels (L: low amplitude impulses, H: high amplitude impulses)

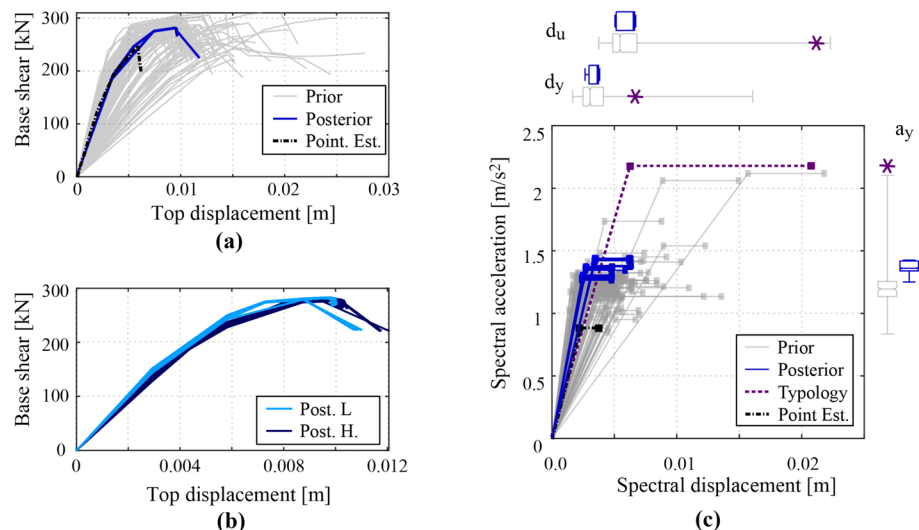


Fig. 13 **a** Prior, Posterior and point estimate pushover curves of building MW1. **b** Posterior pushover curves of building MW1 for low- (L) and high- (H) amplitude impulses. **c** Prior, Posterior and point estimate of the corresponding bilinear capacity curves and comparison with the typological prediction

boxplots. While the average predictions of the prior distributions are close to the posterior ones, the uncertainty range is significantly larger.

Despite the intuitive perception that lower global stiffness, defining the initial part of the pushover curve, leads to reduced lateral capacity, the prior pushover curves do not follow this rule. According to Eq. 1, lower E_{mas} translates to lower compressive strength. Following the hinge definitions formulated by Lagomarsino et al. (2013), lower compressive strength reduces the capacity of the bending-moment hinges, without affecting the capacity of the shear hinges. In cases where the collapse mechanism is governed by the shear capacity of masonry, no clear correlation between E_{mas} and lateral strength exists. Additionally, the soil impedance and slab stiffness affect the global stiffness, while being independent from the strength properties of masonry. Therefore, model configurations with low elastic properties for the soil and the slab may demonstrate reduced global stiffness.

Performance metrics are introduced to analyse the reduction in uncertainty that is achieved with regard to seismic assessment. The considered seismic hazard scenario complies with the Swiss seismic design spectrum for hazard zone 2 and soil class E (SIA 2020). The metrics that are chosen cover the expected hazard level through the displacement demand, the building capacity through the ductility capacity, and the convolution of both through the compliance factor and the ductility demand. The uncertainty distributions of the four metrics are compared in Fig. 14. In order to obtain a point estimate (PE) of the predicted response, which reflects typical engineering assumptions, the 25th percentile of the uncertain ranges for E_{mas} and $G_{tim,eq}$, corresponding to 2.5 GPa, 16.3 MPa, are considered. In addition, fixed boundary conditions are assumed ($G_{soil,eq} \rightarrow \infty$) and all remaining uncertain parameters (see Table 2) are set to average values. Considering the posterior estimates as reference, the PE yields realistic results in terms of DuctC and DispD, yet provides conservative estimates of the DuctD and the CF, indicating an underestimation of the yield force. On the contrary, the typological curve for the studied building, M5.w_M Lagomarsino and Giovinazzi (2006), overestimates both the DuctC and the CF, while underestimates the DuctD, providing overall non-conservative predictions. It should be noted, however, that the typological curve fits rather well the linear part of the lateral load-resisting behavior, despite its generic nature.

A comparison of the posterior pushover curves for low- (PL) versus the high-amplitude (PH) updated EF models, reveals minor differences in the initial stiffness and in the ultimate displacement (see Fig. 13b). Although parameter identification primarily concerns the commonly assumed linear properties of the building, that influence the modal properties that are derived from measurements, the impact of model-updating to the nonlinear seismic response is manifold. Mode shapes define the load pattern of the applied lateral load, the elastic part of the bilinear curve governs the displacement demand and the updated linear parameters are linked to the nonlinear strength (e.g. through Eq. 1). The influence of the amplitude of shaking on the performance metrics is illustrated in the box-plots of Fig. 14. Due to the higher initial stiffness, the PL predictions yield slightly lower DispD. For increasing amplitude the DuctC decreases, which however is compensated by a decrease in DuctD, resulting to almost identical distributions in terms of CF for both amplitude levels.

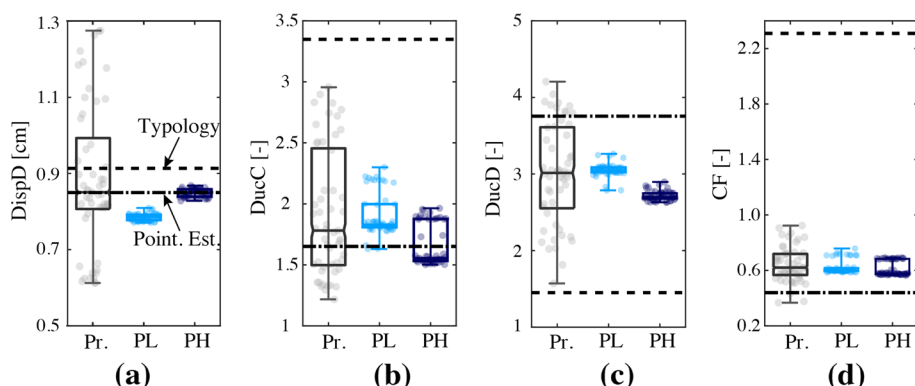


Fig. 14 Prior distributions (Pr.), low-amplitude (PL) and high-amplitude (PH) posterior distributions of performance metrics. The dashed and the dotted-dashed lines indicate the typological prediction and the point estimate respectively

Fig. 15 Identified frequencies and performance metrics of all studied buildings: **a, b** First and second characteristic frequencies, the grey markers indicate the average value of each building. **c, e** Performance metrics based on the prior pushover curves. **d, f** Performance metrics based on the posterior pushover curves

3.2 Analysis of multiple buildings

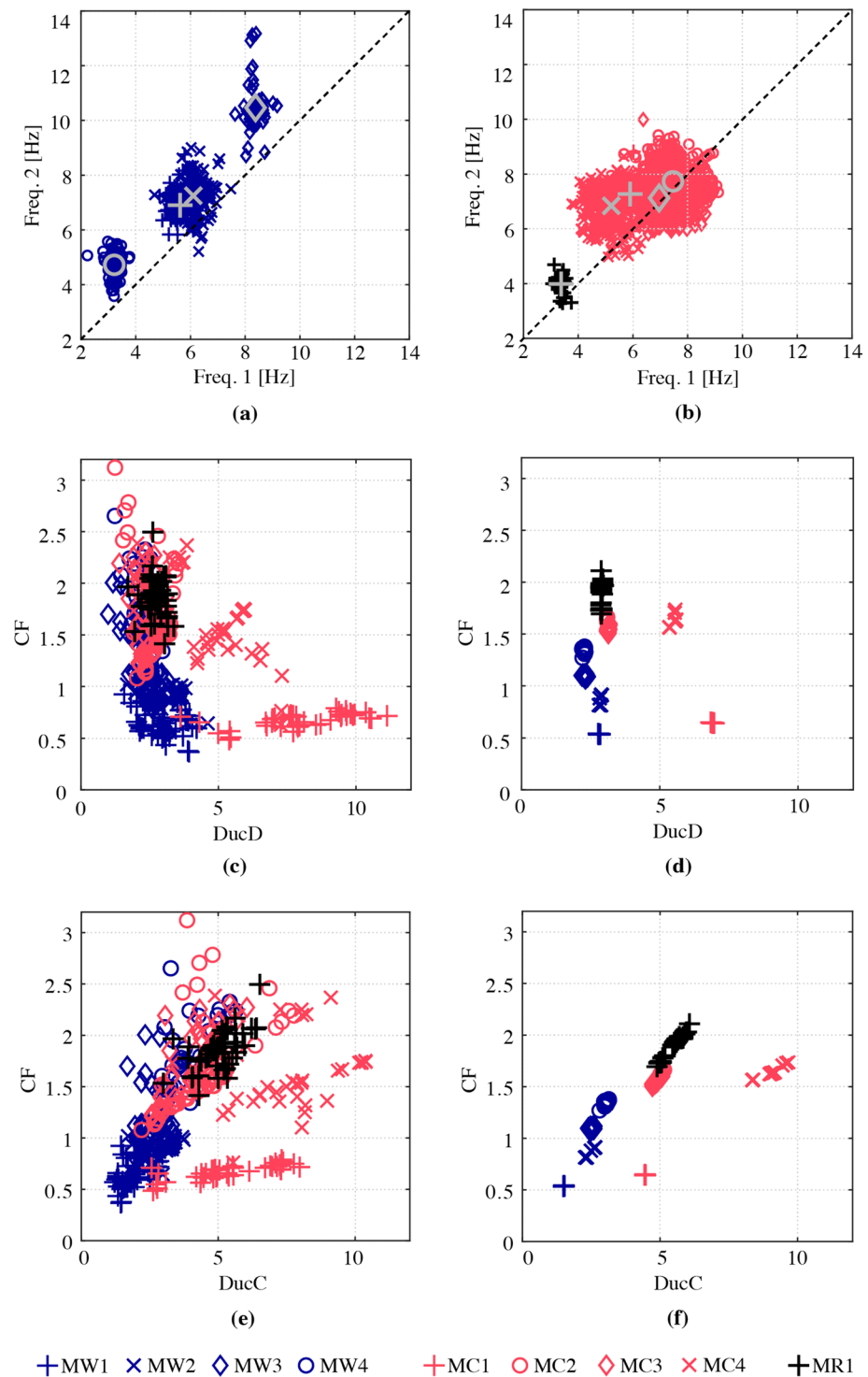
The nine case studies of real masonry buildings, described in Table 3, form a representative subset of existing residential URM buildings in Switzerland. Buildings MW1 to MW4 possess timber slabs and belong to the medium-rise class, with the exception of the low-rise MW3. Buildings MC1 to MC4 have RC floors and fall into the medium-rise typology. The outer dimensions and proportions show significant variability, which is not taken into account in typological classes. Finally, the building MR1 is considered high-rise and contains composite RC-masonry slabs, spanned along the short dimension of the building. All buildings are rather regular in plan and elevation, which is representative of Swiss residential buildings built in the first half of the 20th century.

The identified frequencies of the first translational modal shapes in the two main directions are plotted in Fig. 15a and b for the cases of timber and stiffer slabs. Identified frequencies cover the range between 3 – 14 HZ, which lies in the plateau region of the European seismic design spectra (CEN 2004; SIA 2020). Considering the identification results of individual buildings within each category, the uncertainty in the modal identification, resulting from the variation in direction, amplitude, and duration of impulse responses, demonstrates larger dispersion for the buildings with RC floors. While both stiff and flexible floor buildings show similar variability with respect to the fundamental mode, the buildings with flexible floors demonstrate significantly larger scatter in the second frequency, as well as a clear correlation with the building height. Although MW4 belongs to the medium-rise class, the frequencies lie outside the region of medium-rise buildings, in the vicinity of the high-rise building MR1. Figure 15a and b expose the need for further structural features that are neglected in current typological scheme, such as the amount and distribution of openings, the building age and the local soil conditions, that contribute significantly to the dynamic behaviour of structures. Comparing the frequencies in the two main directions, RC and composite floor buildings show less variability than flexible floor buildings. This can be attributed to the diaphragm-effect of stiff slabs, which is missing in the case of orthotropic flexible timber floors.

Following the workflow described in Sect. 2 and applied in Sect. 3.1, parametric EF models are developed for all studied buildings and model-updating is conducted by means of FSF Bayesian inverse analysis. The seismic performance is evaluated through nonlinear pushover analysis and seismic performance metrics are calculated. Figure 15c to f summarize the performance metrics for the prior and posterior cases for all studied buildings. In the prior case the large scatter of the response predictions hinders any conclusive observation. The posterior plots demonstrate significant uncertainty reduction, which enables a meaningful interpretation of the produced results.

3.2.1 Intra-typological assessment

The behaviour of MC buildings in terms of CF and DucC shows significant scatter. For the given hazard scenario, the CF ranges between 0.6 and 1.7 while the DucC spans between 5 and 10. MC1, which is the oldest building and has the smallest footprint, yields the lowest



CF, while MC4, which is the newest building, produces almost two times higher DucC compared to the other buildings in this class. The DucD is less variable within the class, which, given the low variability in elastic stiffness (see Fig. 15b), implies consistency in terms of yield displacement as well.

Timber floor buildings exhibit less scatter in DucD and DucC, while the CF varies between 0.5 and 1.5. MW1, which is overall the smallest medium-rise building, yields the lowest CF while the largest building (MW4) presents the highest CF in the medium-rise class. Nevertheless, the low-rise building (MW3) reaches the maximum CF of the timber floor category, which is consistent with observations made after recent earthquakes in Italy (D'Amato et al. 2020).

3.2.2 Inter-typological assessment

Despite the intra-typological scatter, the posterior results allow for a comparative discussion of the collective behaviour between different building classes. Overall, timber floor buildings (MW) show inferior seismic performance, yielding lower CF and DucC while being consistently exposed to slightly lower DucD. The low scatter in terms of DucC reflects a more brittle behaviour compared to MC buildings, which is attributed to the inability of flexible orthotropic slabs to redistribute lateral loads. Regarding the composite floor class, although only one building is available, the seismic performance in terms of ductility lies at the intersection between RC and timber floor classes. Composite slabs behave orthotropic and they are lighter and less stiff than conventional RC slabs, while being heavier and stiffer than timber floors. As a result their ability to distribute lateral forces, which correlates with the global structural ductility, is expected to lie between the two classes. MR1 building reaches the highest CF compared to all other buildings, while being the highest and the heaviest building studied. Given that, up to a certain point, structural capacity increases with the acting axial force (see Table 1), the self weight of the building, combined with regularity in plan, has a beneficial influence on the global seismic capacity.

3.2.3 Comparison of updated predictions with typological predictions

Figures 16 and 17 summarize the seismic performance of each individual building, prior to and after model updating, and compare this against the reference performance metrics of the corresponding typology (indicated with a dashed line). The dark lines indicate the posterior estimations and, due to their increased precision and compatibility with measured behavior, the subsequent discussion is focused on posterior distributions.

Overall, the typological curves yield accurate estimates of the DispD, which demonstrates a good approximation of the initial stiffness despite their generic nature. However, they tend to overestimate the CF and the DucC, which can be attributed to the overprediction of the ultimate displacement capacity and the yield force. The global ultimate displacement capacity depends on the nonlinear properties of the model, as well as on the spatial distribution of the bearing elements, which makes their validation at regional scale challenging. Considering best-practice assumptions for the nonlinear behaviour of URM buildings, as described in Sect. 2.1, the posterior results indicate non-conservative estimations from the typological curves. In contrast to DispD, the DucD is consistently underestimated, especially for the case of RC floor buildings. This reflects a misprediction of

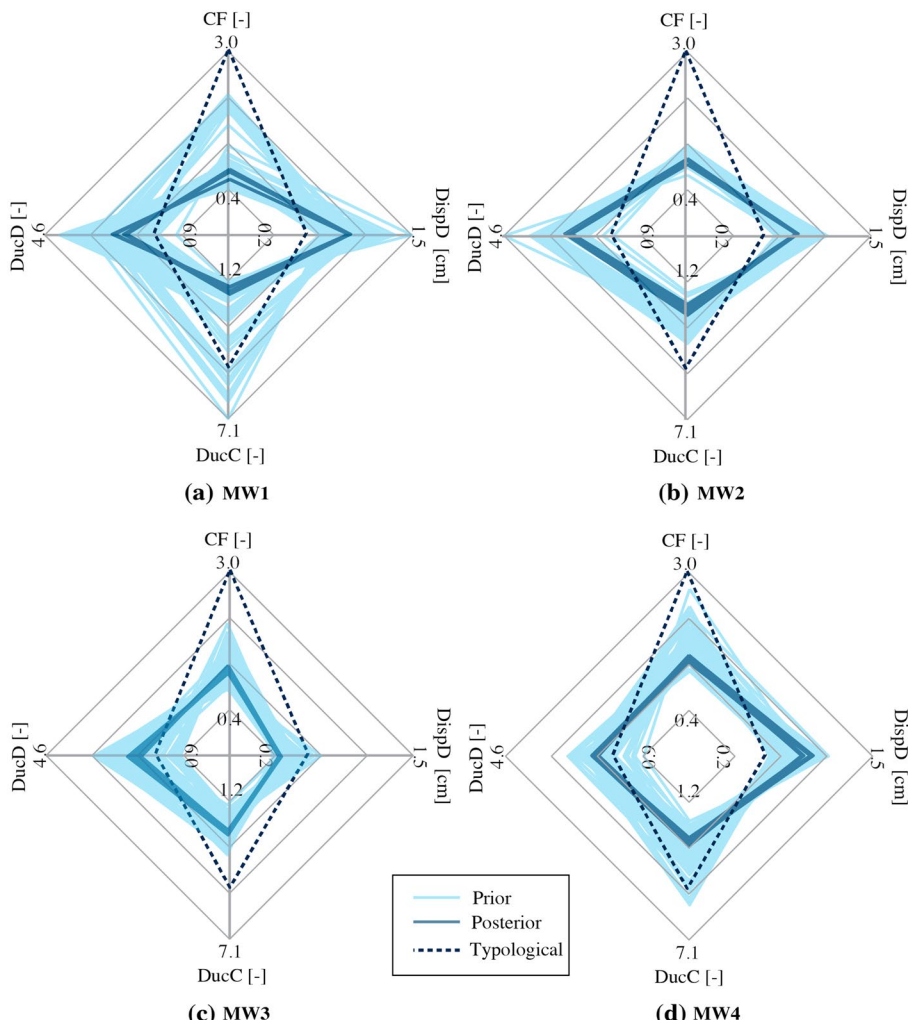


Fig. 16 Performance metrics of timber floor buildings (MW) based on prior and posterior model evaluations and typological predictions

the yield strength, which again relates to the assumptions for the nonlinear parameters at structural element-level.

The underestimation of the DucD is less prominent in the case of timber floor buildings (class M5.w), which implies a better approximation of the yield force. It is mentioned that, according to Lagomarsino and Giovinazzi (2006), this typological class aims to cover “old brick” material, whereas the class M6 that describes RC-floor masonry buildings addresses the corresponding material simply as “masonry” and, due to the appearance of RC floors in later stages than timber floors, may cover newer brick material. Finally, the typological predictions for the DucC is lower than the posterior for the RC floor buildings and higher than the posterior for the timber floor structures. This demonstrates again the inherent incapability of generic typologies to capture building-specific nonlinear metrics that depend

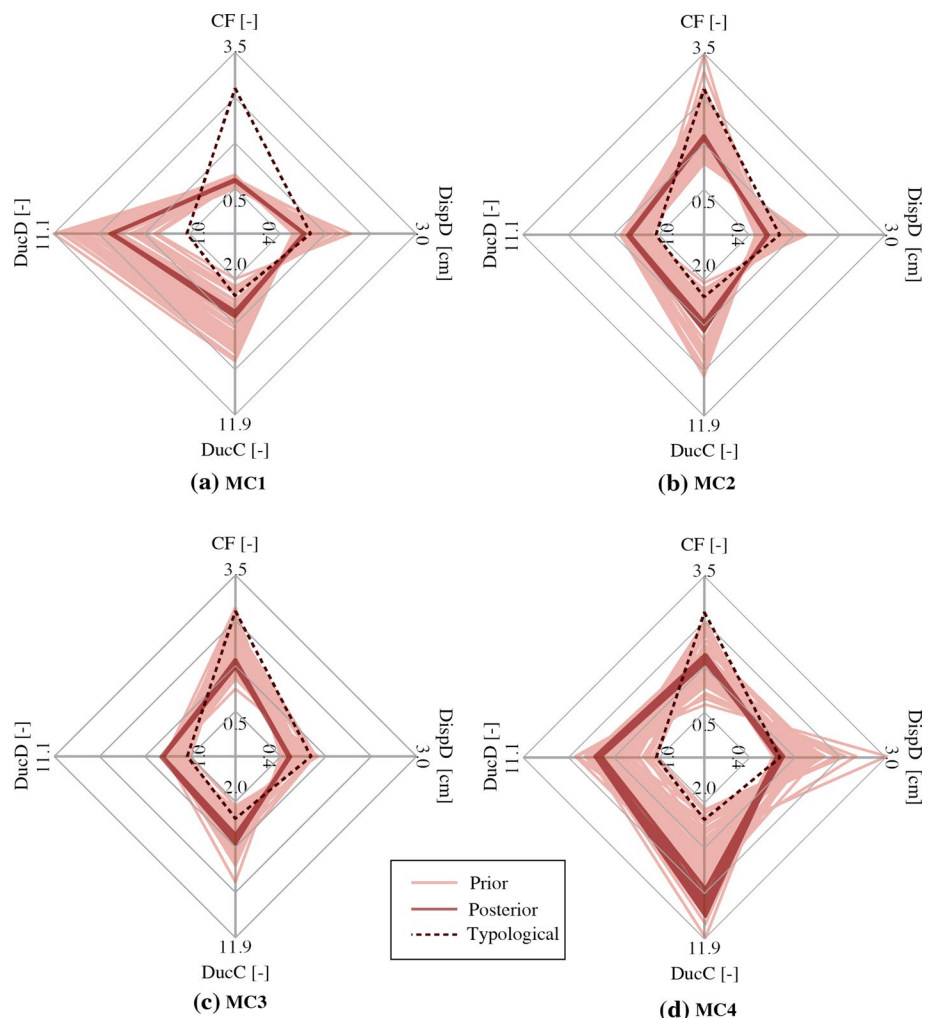


Fig. 17 Performance metrics of RC floor buildings (MC) based on prior and posterior model evaluations and typological predictions

on the redistribution of lateral forces and on the nonlinear behaviour at structural element level for individual buildings. Finally, the results confirm the brittle behaviour of timber floor structures, as well as the beneficial effect of stiff diaphragms on increasing the ductility of such buildings.

4 Conclusions

This paper contains a Bayesian framework for data-driven model-updating, with the aim to reduce uncertainty in seismic performance prediction of multiple URM buildings. Dynamic measurements are fused with EF models representing the physics of URM buildings.

The framework is applied to nine case studies of real URM buildings that form a subset of existing residential buildings in Switzerland and central Europe. It is shown that availability of dynamic measurement data during increased forcing amplitudes, as those enforced during a demolition process, allows to reduce the uncertainty in predicted seismic capacity.

Dynamic measurements at various amplitude levels reveal reversible nonlinear behaviour corresponding to a frequency drop of up to 10%, when compared to the identified frequencies under ambient conditions. BMU facilitates the interpretation of this elastic nonlinearity by attributing it to the strain dependency of soil stiffness and to the elastic modulus of masonry, possibly due to opening and closing of pre-existing cracks.

Contrary to deterministic model-updating techniques, which are prone to over-fitting, BMU succeeds in providing robust estimates, along with information on the underlying distributions of uncertain parameters. The application to nine real case studies indicates that by considering modal shapes in the updating process, BMU reduces model uncertainty by enabling the simultaneous updating of stiffness parameters pertaining to the soil and the superstructure. The propagation of the input uncertainty into the seismic response calculation yields narrow estimates of seismic performance metrics, allowing for comparison of the seismic performance of multiple buildings at typological level.

Masonry structures with RC floors comprise similar behavior until yield displacement, while they exhibit large variability with respect to the ultimate capacity. Timber floor structures show lower scatter and higher vulnerability, both in terms of capacity and ductility, when compared with buildings having stiffer floors. Typological capacity curves capture the initial stiffness of URM buildings, yet overestimate ductility and ultimate capacity. These properties depend on the nonlinear behaviour at the scale of structural elements, as well as on their spatial distribution, hindering the derivation of generally-applicable approximations that rely on generic building properties. The establishment of a refined typology system that is capable of reflecting such distinctions is left as future work.

Appendix: Documentation of Case Studies

The documentation of all case studies is provided in Figs. 18, 19, 20, 21, 22, 23, 24 and 25 as follows: (a) 3D-rendering of the studied structure, (b) typical ground floor including the sensor positions, (c) cross-section of the building.

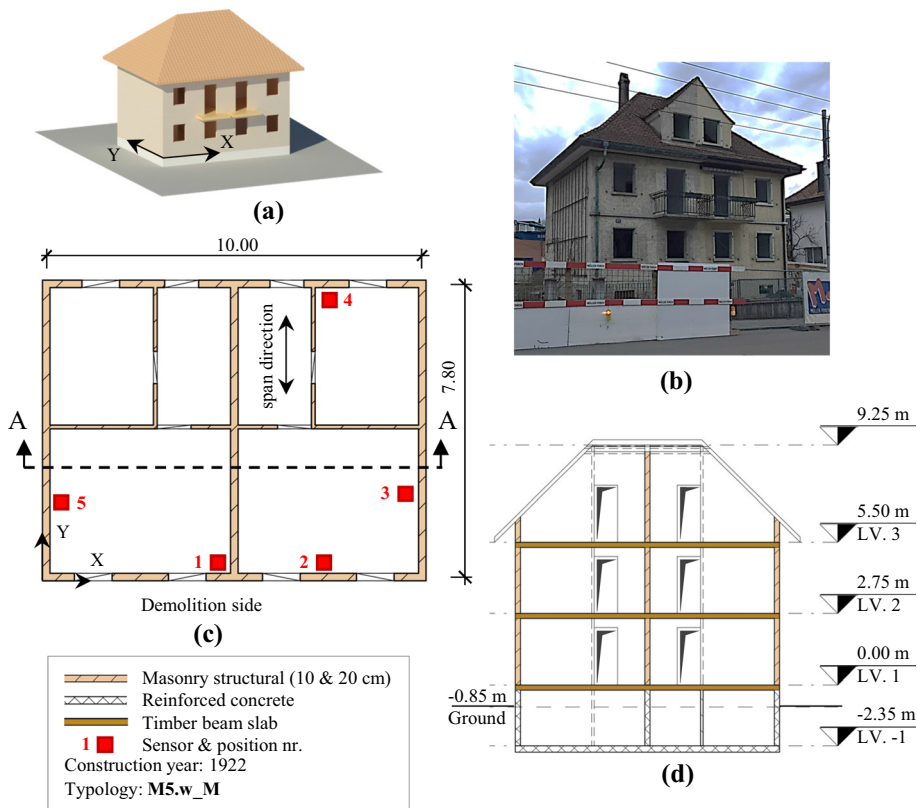


Fig. 18 Case study MW2

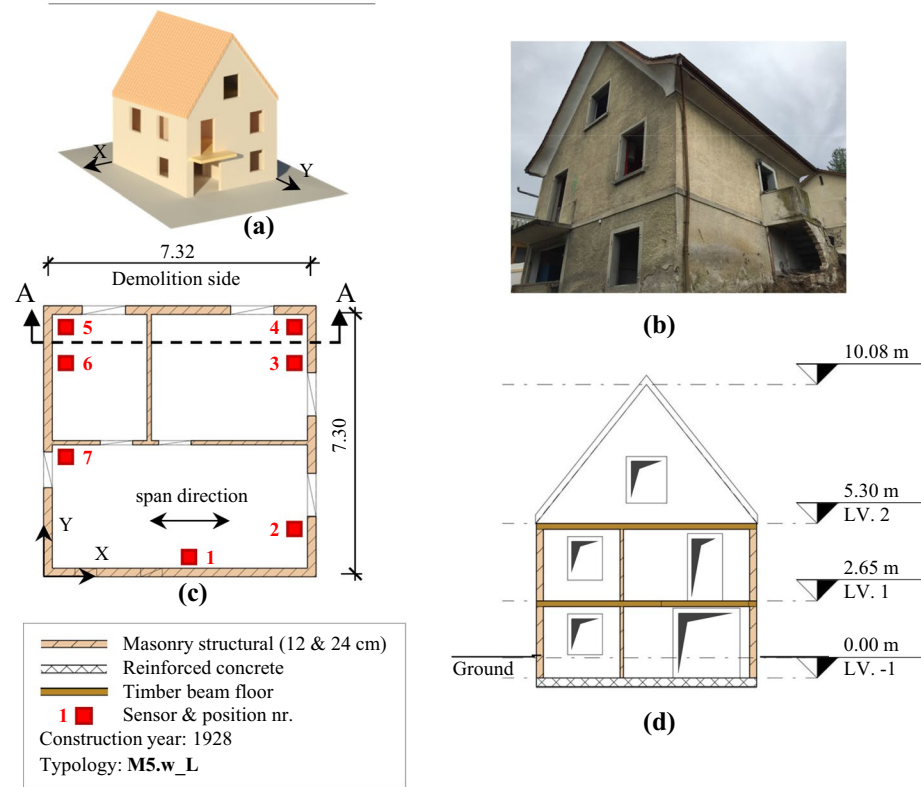


Fig. 19 Case study MW3

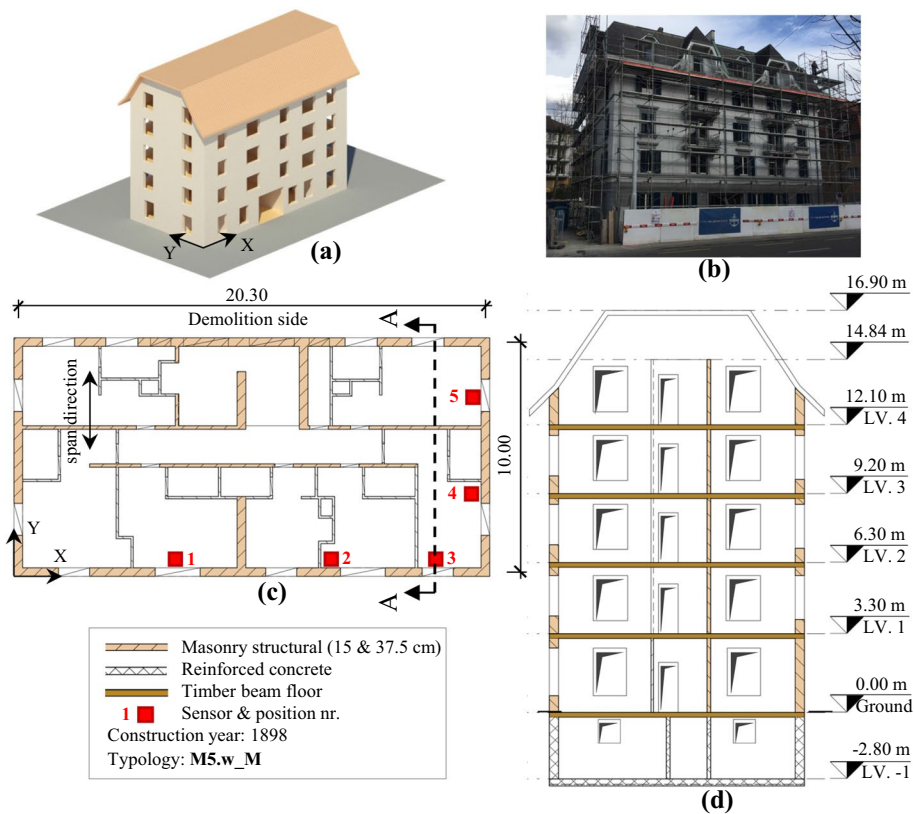


Fig. 20 Case study MW4

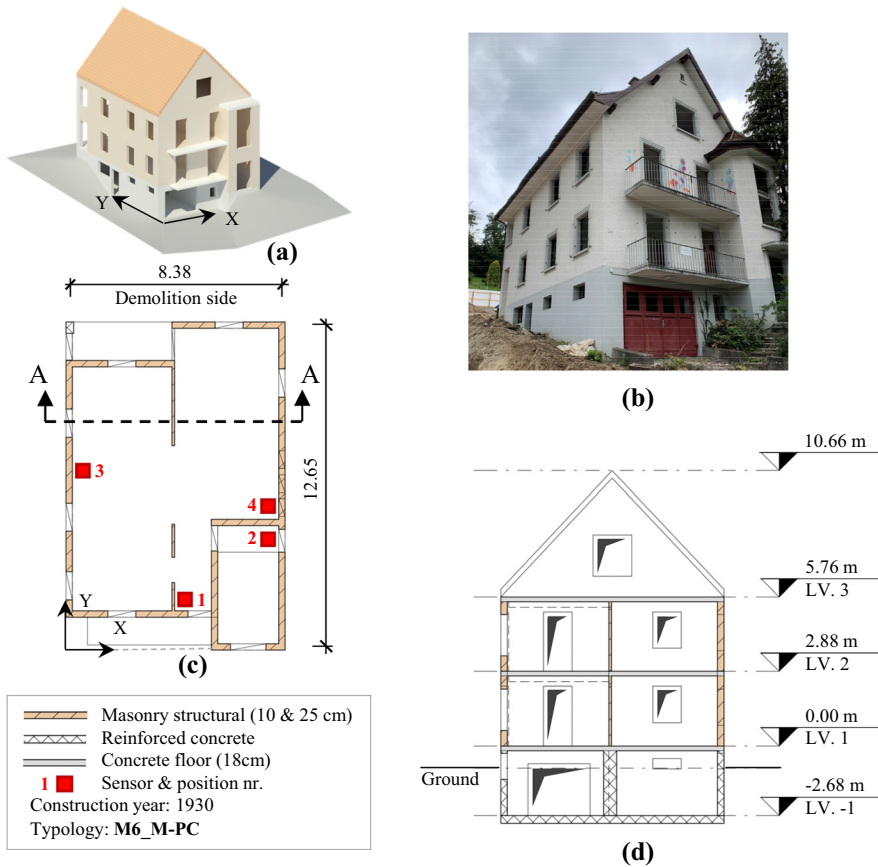


Fig. 21 Case study MC1

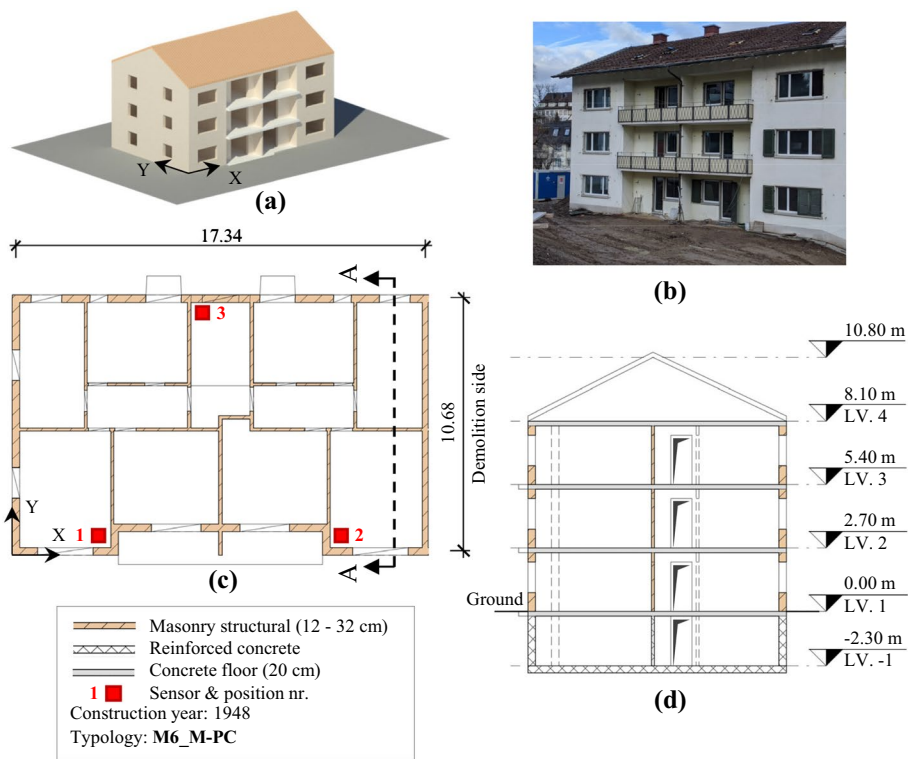


Fig. 22 Case study MC2

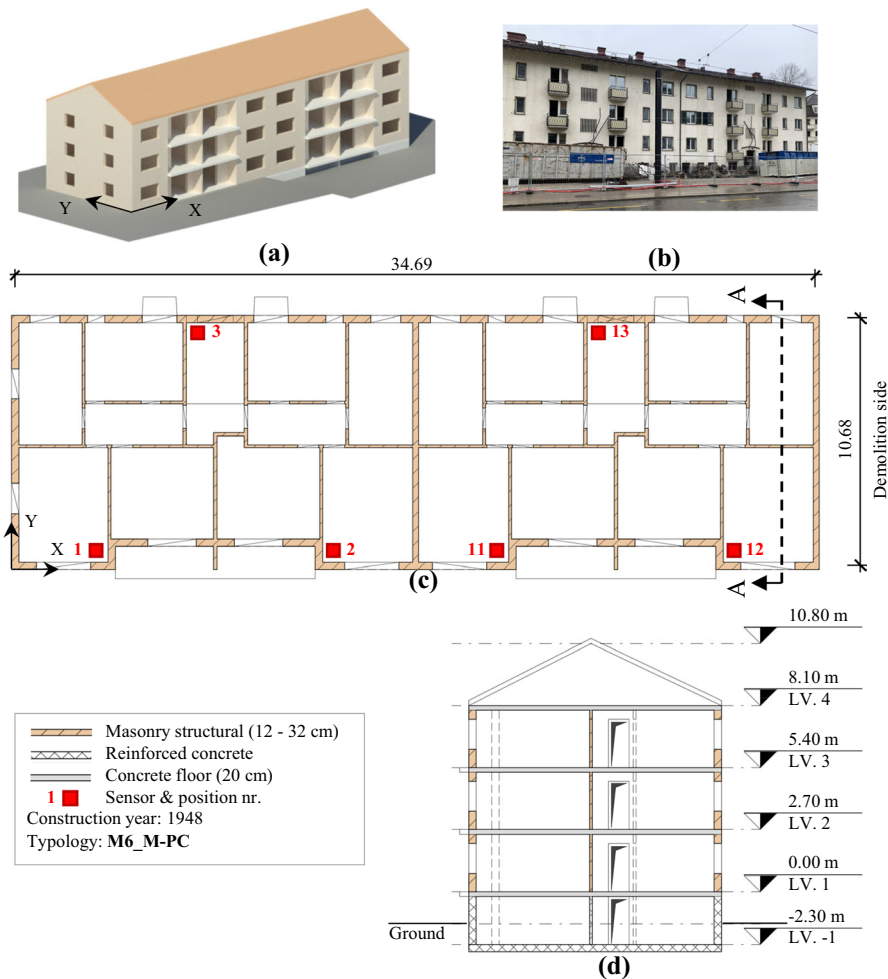


Fig. 23 Case study MC3

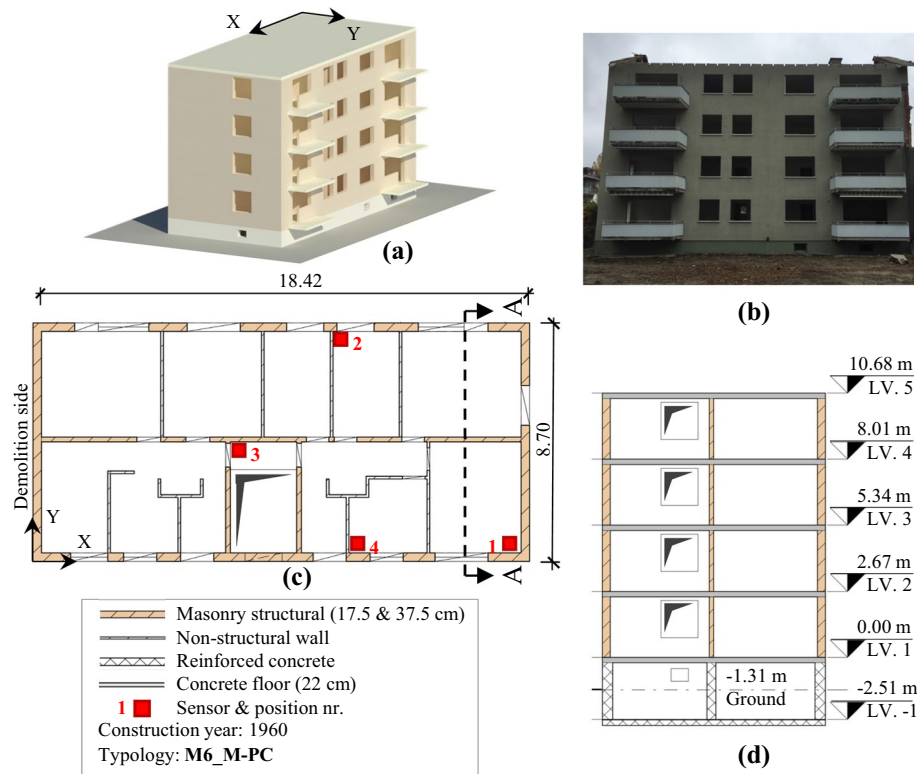


Fig. 24 Case study MC4

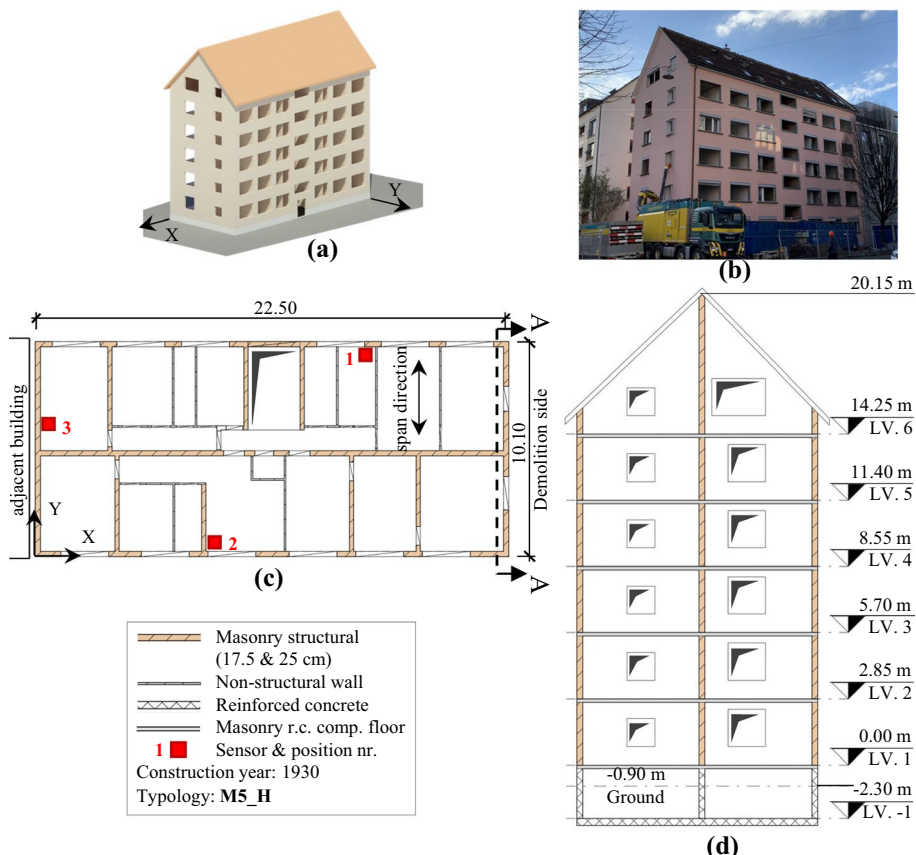


Fig. 25 Case study MR1

Funding Open access funding provided by Swiss Federal Institute of Technology Zurich. The work presented in this paper was financially supported by the Real-time Earthquake Risk Reduction for a Resilient Europe 'RISE' project, financed under the European Union's Horizon 2020 research and innovation program, under grant agreement No 821115, as well as the ETH Risk Center project 'DynaRisk', financed under grant agreement ETH-11 18-1.

Availability of data and material Measurement data and building documentation may be shared on reasonable re-quests to the authors.

Code availability Not applicable.

Declarations

Conflict of interest The authors have no conflicts of interest to declare that are relevant to the content of this article.

Ethical approval Not applicable.

Consent to participate Not applicable.

Consent for publication The authors consent to publish this work in Bulletin of Earthquake Engineering.

Open Access This article is licensed under a Creative Commons Attribution 4.0 International License, which permits use, sharing, adaptation, distribution and reproduction in any medium or format, as long as you give appropriate credit to the original author(s) and the source, provide a link to the Creative Commons licence, and indicate if changes were made. The images or other third party material in this article are included in the article's Creative Commons licence, unless indicated otherwise in a credit line to the material. If material is not included in the article's Creative Commons licence and your intended use is not permitted by statutory regulation or exceeds the permitted use, you will need to obtain permission directly from the copyright holder. To view a copy of this licence, visit <http://creativecommons.org/licenses/by/4.0/>.

References

- ASCE, SEI, (2017) Seismic evaluation and retrofit of existing buildings. American Society of Civil Engineers, USA
- Astorga A, Guégan P, Kashima T (2018) Nonlinear elasticity observed in buildings during a long sequence of earthquakes. *Bullet Seismol Soc Am* 108(3A):1185–1198. <https://doi.org/10.1785/0120170289>
- Bartoli G, Betti M, Marra AM, Monchetti S (2019) A bayesian model updating framework for robust seismic fragility analysis of non-isolated historic masonry towers. *Philos Trans Royal Soc A* 377(2155):20190024. <https://doi.org/10.1098/rsta.2019.0024>
- Beck JL, Au SK (2002) Bayesian updating of structural models and reliability using markov chain monte carlo simulation. *J Eng Mech* 128(4):380–391. [https://doi.org/10.1061/\(ASCE\)0733-9399\(2002\)128:4\(380\)](https://doi.org/10.1061/(ASCE)0733-9399(2002)128:4(380))
- Behmanesh I, Moaveni B, Lombaert G, Papadimitriou C (2015) Hierarchical bayesian model updating for structural identification. *Mech Syst Signal Process* 64:360–376. <https://doi.org/10.1016/j.ymssp.2015.03.026>
- Belmouden Y, Lestuzzi P (2009) An equivalent frame model for seismic analysis of masonry and reinforced concrete buildings. *Constr Build Mater* 23(1):40–53. <https://doi.org/10.1016/j.conbuildmat.2007.10.023>
- Benz T (2007) Small-strain stiffness of soils and its numerical consequences
- Blatman G (2009) Adaptive sparse polynomial chaos expansions for uncertainty propagation and sensitivity analysis. PhD thesis, Université Blaise Pascal, Clermont-Ferrand, France
- Borzi B, Crowley H, Pinho R (2008) Simplified pushover-based earthquake loss assessment (sp-bela) method for masonry buildings. *Int J Architect Herit* 2(4):353–376. <https://doi.org/10.1080/15583050701828178>
- Bracchi S, Rota M, Penna A, Magenes G (2015) Consideration of modelling uncertainties in the seismic assessment of masonry buildings by equivalent-frame approach. *Bullet Earthq Eng* 13(11):3423–3448. <https://doi.org/10.1007/s10518-015-9760-z>
- Cattari S, Giongo I, Marino S, Lin Y, Schiro G, Ingham J, Dizhur D (2015) Numerical simulation of the seismic response of an earthquake damaged urm building. In: New Zealand Society for Earthquake Engineering Technical Conference 2015 Conference
- Çelebi M (2019) S2HM of buildings in USA. Springer International Publishing, Cham, pp 3–30. https://doi.org/10.1007/978-3-030-13976-6_1
- Çelebi M, Haddadi H, Huang M, Valley M, Hooper J, Klemencic R (2019) The behavior of the salesforce tower, the tallest building in San Francisco, California inferred from Earthquake and ambient shaking. *Earthq Spectra* 35(4):1711–1737. <https://doi.org/10.1193/112918EQS273M>
- CEN (2004) EN 1998–1: 2004 Eurocode 8: Design of structures for earthquake resistance-Part 1: general rules, seismic actions and rules for buildings. Comité Européen de Normalisation, Bruxelles
- CEN (2005) EN 1998–3: 2005 Eurocode 8: Design of structures for earthquake resistance-Part 3: assessment and retrofitting of buildings. Comité Européen de Normalisation, Bruxelles
- Ceravolo R, Matta E, Quattrone A, Zanotti Fragonara L (2017) Amplitude dependence of equivalent modal parameters in monitored buildings during earthquake swarms. *Earthq Eng Struct Dyn* 46(14):2399–2417. <https://doi.org/10.1002/eqe.2910>
- Civera M, Calamai G, Zanotti Fragonara L (2021) System identification via fast relaxed vector fitting for the structural health monitoring of masonry bridges. *Structures* 30:277–293. <https://doi.org/10.1016/j.istruc.2020.12.073>
- Crowley H, Rodrigues D, Silva V, Despotaki V, Romão X, Castro JM, Akkar S, Hancilar U, Pitilakis K, Pitilakis D, et al. (2018) Towards a uniform earthquake risk model for europe. In: 16th European Conference on Earthquake Engineering

- Diana L, Manno A, Lestuzzi P, Podestà S, Luchini C (2018) Impact of displacement demand reliability for seismic vulnerability assessment at an urban scale. *Soil Dyn Earthq Eng* 112:35–52. <https://doi.org/10.1016/j.soildyn.2018.05.002>
- Diana L, Lestuzzi P, Podestà S, Luchini C (2019) Improved urban seismic vulnerability assessment using typological curves and accurate displacement demand prediction. *J Earthq Eng*. <https://doi.org/10.1080/13632469.2019.1597784>
- Diana L, Manno A, Lestuzzi P (2019) Seismic displacement demand prediction in non-linear domain: optimization of the n2 method. *Earthq Eng Eng Vibr* 18(1):141–158. <https://doi.org/10.1007/s11803-019-0495-8>
- Diana L, Thiriot J, Reuland Y, Lestuzzi P (2019) Application of association rules to determine building typological classes for seismic damage predictions at regional scale: the case study of basel. *Front Built Environ* 5:51. <https://doi.org/10.3389/fbuil.2019.00051>
- D'Amato M, Laguardia R, Di Trocchio G, Coltellacci M, Gigliotti R (2020) Seismic risk assessment for masonry buildings typologies from l'aquila 2009 earthquake damage data. *J Earthq Eng*. <https://doi.org/10.1080/13632469.2020.1835750>
- da Porto F, Donà M, Rosti A, Rota M, Lagomarsino S, Cattari S, Borzi B, Onida M, De Gregorio D, Perelli FL, et al. (2021) Comparative analysis of the fragility curves for italian residential masonry and rc buildings. *Bulletin of Earthquake Engineering* pp 1–44
- Ercan E (2018) Assessing the impact of retrofitting on structural safety in historical buildings via ambient vibration tests. *Constr Build Mater* 164:337–349. <https://doi.org/10.1016/j.conbuildmat.2017.12.154>
- Fajfar P (2000) A nonlinear analysis method for performance-based seismic design. *Earthq spectra* 16(3):573–592. <https://doi.org/10.1193/1.1586128>
- Fajfar P, Fischinger M (1988) N2-a method for non-linear seismic analysis of regular buildings. *Proc Ninth World Conf Earthq Eng* 5:111–116
- Foti D, Diaferio M, Giannoccaro NI, Mongelli M (2012) Ambient vibration testing, dynamic identification and model updating of a historic tower. *NDT & e Int* 47:88–95. <https://doi.org/10.1016/j.ndteint.2011.11.009>
- García-Macías E, Ierimonti L, Venanzi I, Ubertini F (2021) An innovative methodology for online surrogate-based model updating of historic buildings using monitoring data. *Int J Architect Herit* 15(1):92–112. <https://doi.org/10.1080/15583058.2019.1668495>
- Gazetas G (1991) Formulas and charts for impedances of surface and embedded foundations. *J Geotech Eng* 117:1363–1381. [https://doi.org/10.1061/\(ASCE\)0733-9410\(1991\)117:9\(1363\)](https://doi.org/10.1061/(ASCE)0733-9410(1991)117:9(1363))
- Girardi M, Padovani C, Pellegrini D, Robol L (2021) A finite element model updating method based on global optimization. *Mech Syst Signal Process* 152:107372. <https://doi.org/10.1016/j.ymssp.2020.107372>
- Goodman J, Weare J (2010) Ensemble samplers with affine invariance. *Commun Appl Math Comput Sci* 5(1):65–80. <https://doi.org/10.2140/camcos.2010.5.65>
- Grünthal G (1998) European macroseismic scale 1998. Tech. rep, European Seismological Commission (ESC)
- Guéguen P, Brossault MA, Roux P, Singaudo JC (2020) Slow dynamics process observed in civil engineering structures to detect structural heterogeneities. *Eng Struct* 202:109833
- Jaiswal K, Wald D, Porter K (2010) A global building inventory for earthquake loss estimation and risk management. *Earthq Spectra* 26(3):731–748. <https://doi.org/10.1193/1.3450316>
- Juang JN, Pappa RS (1985) An eigensystem realization algorithm for modal parameter identification and model reduction. *J Guidance, Control, Dyn* 8(5):620–627
- Lagomarsino S, Giovinazzi S (2006) Macroseismic and mechanical models for the vulnerability and damage assessment of current buildings. *Bullet Earthq Eng* 4(4):415–443. <https://doi.org/10.1007/s10518-006-9024-z>
- Lagomarsino S, Penna A, Galasco A, Cattari S (2013) TREMURI program: an equivalent frame model for the nonlinear seismic analysis of masonry buildings. *Eng Struct* 56:1787–1799. <https://doi.org/10.1016/j.engstruct.2013.08.002>
- Lang K, Bachmann H (2004) On the seismic vulnerability of existing buildings: a case study of the city of basel. *Earthq Spectra* 20(1):43–66. <https://doi.org/10.1193/1.1648335>
- Lestuzzi P, Podestà S, Luchini C, Garofano A, Kazantzidou-Firtinidou D, Bozzano C (2017) Validation and improvement of risk-ue lm2 capacity curves for urm buildings with stiff floors and rc shear walls buildings. *Bullet Earthq Eng* 15(3):1111–1134. <https://doi.org/10.1007/s10518-016-9981-9>
- Limoncelli M (2010) Frequency response function interpolation for damage detection under changing environment. *Mech Syst Signal Process* 24(8):2898–2913. <https://doi.org/10.1016/j.ymssp.2010.03.004>

- Limongelli MP, Dolce M, Spina D, Guéguen P, Langlais M, Wolinieck D, Maufroy E, Karakostas CZ, Lekidis VA, Morfidis K, Salonikios T, Rovithis E, Makra K, Masciotta MG, Lourenço PB (2019) S2HM in some European Countries. Springer International Publishing, Cham, pp 303–343. https://doi.org/10.1007/978-3-030-13976-6_13
- Lulić L, Ožić K, Kišiček T, Hafner I, Stepinac M (2021) Post-earthquake damage assessment-case study of the educational building after the zagreb earthquake. *Sustainability* 13(11):6353
- Manzini CF, Ottонelli D, Degli Abbati S, Marano C, Cordasco EA (2021) Modelling the seismic response of a 2-storey urn benchmark case study: comparison among different equivalent frame models. *Bullet Earthq Eng.* <https://doi.org/10.1007/s10518-021-01173-2>
- Marelli S, Sudret B (2014) UQLab: a framework for uncertainty quantification in Matlab, pp 2554–2563. <https://doi.org/10.1061/9780784413609.257>
- Marelli S, Sudret B (2019) UQLab user manual - Polynomial chaos expansions. Tech. rep, Chair of Risk, Safety and Uncertainty Quantification, ETH Zurich, Switzerland
- Martakis P, Taeseri D, Chatzi E, Laue J (2017) A centrifuge-based experimental verification of soil-structure interaction effects. *Soil Dyn Earthq Eng* 103:1–14. <https://doi.org/10.1016/j.soildyn.2017.09.005>
- Martakis P, Reuland Y, Chatzi E (2021) Amplitude-dependent model updating of masonry buildings undergoing demolition. *Smart Struct Syst.* <https://doi.org/10.12989/sss.2021.27.2.157>
- Martakis P, Reuland Y, Chatzi E, Engineering G (2021b) Data-driven model updating for seismic assessment of existing buildings. In: 10th SHIMII conference proceedings, Porto
- MBIE-NZSEE, The seismic assessment of existing buildings. New Zealand Society for Earthquake Engineering, New Zealand, (2017)
- McKay MD, Beckman RJ, Conover WJ (1979) A comparison of three methods for selecting values of input variables in the analysis of output from a computer code. *Technometrics* 21(2):239–245. <https://doi.org/10.2307/1268522>
- Michel C, Guéguen P, Bard PY (2008) Dynamic parameters of structures extracted from ambient vibration measurements: an aid for the seismic vulnerability assessment of existing buildings in moderate seismic hazard regions. *Soil Dyn Earthq Eng* 28(8):593–604. <https://doi.org/10.1016/j.soildyn.2007.10.002>
- Michel C, Zapico B, Lestuzzi P, Molina FJ, Weber F (2011) Quantification of fundamental frequency drop for unreinforced masonry buildings from dynamic tests. *Earthq Eng Struct Dyn* 40(11):1283–1296. <https://doi.org/10.1002/eqe.1088>
- Michel C, Crowley H, Hannewald P, Lestuzzi P, Fäh D (2018) Deriving fragility functions from bilinearized capacity curves for earthquake scenario modelling using the conditional spectrum. *Bullet Earthq Eng* 16(10):4639–4660. <https://doi.org/10.1007/s10518-018-0371-3>
- Michel C, Karbassi A, Lestuzzi P (2018) Evaluation of the seismic retrofitting of an unreinforced masonry building using numerical modeling and ambient vibration measurements. *Eng Struct* 158:124–135. <https://doi.org/10.1016/j.engstruct.2017.12.016>
- Milutinovic ZV, Trendafiloski GS (2003) Risk-ue an advanced approach to earthquake risk scenarios with applications to different european towns. Contract: EVK4-CT-2000-00014, WP4: Vulnerability of Current Buildings pp 1–111, https://doi.org/10.1007/978-1-4020-3608-8_23
- Ministero delle Infrastrutture e dei trasporti (2018) NTC 2018: D.M. del Ministero delle Infrastrutture e dei trasporti del 17/01/2018. Aggiornamento delle Norme Tecniche per le Costruzioni (in Italian) p 198
- Nakamura Y, Derakhshan H, Sheikh A, Ingham J, Griffith M (2016) Equivalent frame modelling of an unreinforced masonry building with flexible diaphragms: a case study. *Bullet New Zealand Soc Earthq Eng* 49(3):234–244. <https://doi.org/10.5459/bnzsee.49.3.234-244>
- Nozari A, Behmanesh I, Yousefianmoghadam S, Moaveni B, Stavridis A (2017) Effects of variability in ambient vibration data on model updating and damage identification of a 10-story building. *Eng Struct* 151:540–553. <https://doi.org/10.1016/j.engstruct.2017.08.044>
- OPCM (2003) OPCM3274: code for the seismic design, assessment and retrofitting of buildings (in Italian). OPCM, Italy
- Oropeza M, Michel C, Lestuzzi P (2010) A simplified analytical methodology for fragility curves estimation in existing buildings. In: 14th European Conference of Earthquake Engineering (ECEE), vol 600
- Pai SG, Reuland Y, Smith IF (2019) Data-interpretation methodologies for practical asset-management. *J Sens Actuat Netw* 8(2):36. <https://doi.org/10.3390/jsan8020036>
- Parisse F, Cattari S, Marques R, Lourenco P, Magenes G, Beyer K, Calderoni B, Camata G, Cordasco E, Erberik M et al (2021) Benchmarking the seismic assessment of unreinforced masonry buildings from a blind prediction test. *Structures* 31:982–1005
- Pasticier L, Amadio C, Fragiocomo M (2008) Non-linear seismic analysis and vulnerability evaluation of a masonry building by means of the SAP2000 vol 10 code. *Earthq Eng Struct Dyn* 37(3):467–485. <https://doi.org/10.1002/eqe.770>

- Peeters B, De Roeck G (1999) Reference-based stochastic subspace identification for output-only modal analysis. *Mech Syst Signal Process* 13(6):855–878. <https://doi.org/10.1006/mssp.1999.1249>
- Quagliarini E, Maracchini G, Clementi F (2017) Uses and limits of the equivalent frame model on existing unreinforced masonry buildings for assessing their seismic risk: A review. *J Build Eng* 10:166–182. <https://doi.org/10.1016/j.jobe.2017.03.004>
- Reuland Y, Lestuzzi P, Smith IF (2017) Data-interpretation methodologies for non-linear earthquake response predictions of damaged structures. *Front Built Environ* 3:43. <https://doi.org/10.3389/fbuil.2017.00043>
- Riedel I, Guéguen P, Dalla Mura M, Pathier E, Leduc T, Chanussot J (2015) Seismic vulnerability assessment of urban environments in moderate-to-low seismic hazard regions using association rule learning and support vector machine methods. *Nat Hazards* 76(2):1111–1141. <https://doi.org/10.1007/s11069-014-1538-0>
- Sabia D, Aoki T, Cosentini RM, Lancellotta R (2015) Model updating to forecast the dynamic behavior of the ghirlandina tower in modena, italy. *J Earthq Eng* 19(1):1–24. <https://doi.org/10.1080/13632469.2014.962668>
- Schafer RW (2011) What is a savitzky-golay filter [lecture notes]. *IEEE Signal Process Mag* 28(4):111–117. <https://doi.org/10.1109/MSP.2011.941097>
- SIA (2017) SIA 269/8 Erhaltung von Tragwerken - Erdbeben (Maintenance of Structures - Earthquakes). SIA, Zurich
- SIA (2020) SIA 261 Einwirkungen auf Tragwerke (Structural loads). SIA, Zurich
- Snoj J, Österreicher M, Dolšek M (2013) The importance of ambient and forced vibration measurements for the results of seismic performance assessment of buildings obtained by using a simplified non-linear procedure: Case study of an old masonry building. *Bullet Earthq Eng* 11(6):2105–2132. <https://doi.org/10.1007/s10518-013-9494-8>
- Sobol I (2001) Global sensitivity indices for nonlinear mathematical models and their monte carlo estimates. *Math Comput Simul* 55(1):271–280. [https://doi.org/10.1016/S0378-4754\(00\)00270-6](https://doi.org/10.1016/S0378-4754(00)00270-6)
- Song M, Behmanesh I, Moaveni B, Papadimitriou C (2019) Modeling error estimation and response prediction of a 10-story building model through a hierarchical bayesian model updating framework. *Front Built Environ* 5:7. <https://doi.org/10.3389/fbuil.2019.00007>
- Song M, Moaveni B, Papadimitriou C, Stavridis A (2019) Accounting for amplitude of excitation in model updating through a hierarchical bayesian approach: application to a two-story reinforced concrete building. *Mech Syst Signal Process* 123:68–83. <https://doi.org/10.1016/j.ymssp.2018.12.049>
- Soti R, Abdulrahman L, Barbosa AR, Wood RL, Mohammadi ME, Olsen MJ (2020) Case study: post-earthquake model updating of a heritage pagoda masonry temple using aem and fem. *Eng Struct* 206:109950. <https://doi.org/10.1016/j.engstruct.2019.109950>
- Soyoz S (2019) Model updating techniques for structures under seismic excitation. Springer International Publishing, Cham, pp 199–216. https://doi.org/10.1007/978-3-030-13976-6_8
- Spina D, Acunzo G, Fiorini N, Mori F, Dolce M (2019) A probabilistic simplified seismic model of masonry buildings based on ambient vibrations. *Bullet Earthq Eng* 17(2):985–1007. <https://doi.org/10.1007/s10518-018-0481-y>
- Standoli G, Salachoris GP, Masciotta MG, Clementi F (2021) Modal-based fe model updating via genetic algorithms: exploiting artificial intelligence to build realistic numerical models of historical structures. *Constr Build Mater* 303:124393
- Straub D, Papaioannou I (2015) Bayesian updating with structural reliability methods. *J Eng Mech* 141(3):04014134. [https://doi.org/10.1061/\(ASCE\)EM.1943-7889.0000839](https://doi.org/10.1061/(ASCE)EM.1943-7889.0000839)
- Sudret B (2008) Global sensitivity analysis using polynomial chaos expansions. *Reliability Eng Syst Saf* 93(7):964–979. <https://doi.org/10.1016/j.ress.2007.04.002>
- Tarantola A (2006) Popper, bayes and the inverse problem. *Nat Phys* 2(8):492–494. <https://doi.org/10.1038/nphys375>
- Torres W, Almazán JL, Sandoval C, Boroschek R (2017) Operational modal analysis and fe model updating of the metropolitan cathedral of santiago, chile. *Eng Struct* 143:169–188. <https://doi.org/10.1016/j.engstruct.2017.04.008>

Authors and Affiliations

Panagiotis Martakis¹  · Yves Reuland¹ · Marco Imesch¹ · Eleni Chatzi¹

Yves Reuland
reuland@ibk.baug.ethz.ch

Marco Imesch
imeschm@student.ethz.ch

Eleni Chatzi
chatzi@ibk.baug.ethz.ch

¹ ETH Zurich Department of Civil Environmental and Geomatic Engineering: Eidgenössische Technische Hochschule Zurich Departement Bau Umwelt und Geomatik, Zurich, Switzerland